A moist available potential energy budget for an axisymmetric tropical cyclone

A Moist Available Potential Energy Budget for an Axisymmetric Tropical Cyclone

Bethan L. Harris,[a,b] Rémi Tailleux,[a] Christopher E. Holloway,[a] Pier Luigi Vidale,[c]

[a] *Department of Meteorology, University of Reading, Reading, United Kingdom*

[b] *UK Centre for Ecology & Hydrology, Wallingford, United Kingdom*

[c] *National Centre for Atmospheric Science, Department of Meteorology, University of Reading, Reading, United Kingdom*

Corresponding author: Rémi Tailleux, r.g.j.tailleux@reading.ac.uk

ABSTRACT: The main energy source for the intensification of a tropical cyclone (TC) is widely accepted to be the transfer of energy from the ocean to the atmosphere via surface fluxes. The pathway through which these surface fluxes lead to an increase in the kinetic energy of the cyclone has typically been interpreted either in terms of total potential energy, dry Available Potential Energy (APE), or through the entropy-based heat engine viewpoint. Here, we use the local theory of APE to construct a budget of moist APE for an idealised axisymmetric simulation of a tropical cyclone. This is the first full budget of local moist APE budget for an atmospheric model. In the local moist APE framework, latent surface heat fluxes are the dominant generator of moist APE, which is then converted into kinetic energy via buoyancy fluxes. In the core region of the TC, the inward transport of APE by the secondary circulation is more important than its local production. The APE viewpoint describes spatially- and temporally-varying efficiencies; these may be useful in understanding how changes in efficiency influence TC development, and have a maximum that can be linked to the Carnot efficiency featuring in potential intensity theory.

1. Introduction

Current high-resolution global climate models (also known as general circulation models, or GCMs) are capable of reproducing to a reasonable degree the global frequency of TCs and the spatial distribution of TC track density (Shaevitz et al. 2014; Roberts et al. 2015, 2020). However, the distribution of TC intensity is more difficult to capture, since intensity is influenced by processes at many scales, from inner-core mixing to convection to the interaction of the core with its environment (Marks et al. 1998), some of which occur at much finer scales than GCM resolution.

Different climate models can produce very different distributions of tropical cyclone (TC) intensity, even when their horizontal resolutions are similar (Shaevitz et al. 2014). Aspects of model configuration that have been shown to affect TC intensity in GCMs include the horizontal resolution (Manganello et al. 2012; Shaevitz et al. 2014; Roberts et al. 2015, 2020), the convective parameterisation (Reed and Jablonowski 2011; Kim et al. 2012; Murakami et al. 2012a,b; Stan 2012; Zhao et al. 2012; Lim et al. 2015), the dynamical core (Reed et al. 2015) and atmosphere-ocean coupling (Zarzycki 2016). Similar changes in projected TC distributions can occur for different physical reasons. For example, introducing stochastic physics to a GCM can result in an increase in TC frequency that is approximately equivalent to a 50% increase in resolution; whereas the higher frequency in the case of increased resolution is primarily due to reduced vertical wind shear, the stochastic physics increases the frequency by moistening the mid-troposphere (Vidale et al. 2021).

This makes it challenging to understand the best routes to developing numerical models that can accurately represent the intensification and maximum intensity of TCs for the correct physical reasons. There has therefore been a recent effort to design process-oriented diagnostics for TCs in GCMs (Kim et al. 2018; Wing et al. 2019; Moon et al. 2019), in order to investigate the mechanisms by which a model's configuration choices lead to differences in the intensity of its TCs. Kim et al. (2018) identified that the representation of moisture, convection and the coupling between them are important factors in the intensity of TCs produced by climate models.

A natural way to explore the links between moist processes, convection and intensification in modelled TCs is through the use of an energy budget as a diagnostic tool. Previous energy budgets of TCs have been mostly based on total potential energy, dry APE or entropy frameworks. This paper will develop a novel energy budget, based on local moist available potential energy (APE)

theory, for a simple axisymmetric TC model. Moist APE theory is advantageous for studying TC intensification because it is designed to directly link the production of available energy by diabatic processes and the ultimate development of the TC via the generation of kinetic energy, and it fully incorporates the effects of moisture-convection coupling. It is also expected that surface fluxes are a key source of moist APE (Pauluis 2007; Tang and Emanuel 2012; Wong et al. 2016), whereas in total potential energy or dry APE frameworks, latent heat release above the boundary layer is treated as the major source of energy for the TC. This means that a moist APE budget is likely to be more useful for studying the effects of boundary layer processes on the energetics; these processes are known to be important to TC intensification (Persing et al. 2013; Kilroy et al. 2016; Schmidt and Smith 2016).

Since this is the first full budget of moist APE for the atmosphere, we focus on a simple, idealised TC model, so that the fundamental properties of the budget can be established in a setting where all processes can be accounted for to ensure budget closure. We construct and analyse the moist local APE budget for a TC simulated by the axisymmetric model of Rotunno and Emanuel (1987), suggest how such a budget could provide useful diagnostic information for more complex models, and discuss its advantages over previous energetic approaches.

The concept of APE was introduced by Lorenz (1955), who defined it as the portion of the total potential energy (TPE = internal + gravitational potential energy) in the atmosphere that can be converted into kinetic energy by adiabatic motions. It can be seen that not all TPE is APE by considering a stable atmosphere with a horizontal density stratification. In this case, no atmospheric motion is expected, so the APE is zero, but the atmosphere still contains TPE. Lorenz defined the APE of the atmosphere as the difference in TPE between its actual state and the state of minimum TPE that could be achieved by rearranging it through adiabatic motion. This minimised potential energy state is known as the *reference state*. The TPE contained in the atmosphere in its reference state is the Background Potential Energy (BPE); Lorenz's method partitions the TPE into APE and BPE. However, there are a number of drawbacks to using Lorenz APE to study TC intensification. The rearrangement-based reference state means that the theory is globally rather than locally defined; it is therefore not clear how the spatial distribution of kinetic energy production can be investigated. For the moist atmospheric case, the reference state is also difficult to obtain, due to the possibility of latent heat release during rearrangement (Lorenz 1978). No analytical method exists

to calculate Lorenz APE in a moist atmosphere. Various sorting algorithms have been developed to approximate it (Lorenz 1979; Randall and Wang 1992; Wong et al. 2016; Stansifer et al. 2017), but these heuristic approaches often make it difficult to understand the physical source of the APE (Harris and Tailleux 2018).

An alternative form of APE theory is the local APE defined by Andrews (1981); Holliday and McIntyre (1981). In local APE theory, each moist air parcel's APE density is computed independently of the other parcels', rather than employing a Lorenzian domain-wide rearrangement. Any hydrostatically-balanced atmospheric state may be chosen as the reference state. The parcel's nearest level of neutral buoyancy (LNB) is computed with respect to that reference state. Its APE density is then defined as the work that must be done by buoyancy forces on the parcel to bring it reversibly and adiabatically from this LNB in the reference state to its actual position. The APE thus gives the total potential energy of the parcel that can be converted into kinetic energy by reversible adiabatic motion through the reference state.

This is similar to the concept of Convective Available Potential Energy (CAPE), which is also defined as an integral of buoyancy from a parcel's actual height to its LNB (e.g. Emanuel 1994, p. 169). The main difference between the two is that when defining CAPE, the parcel's buoyancy is calculated relative to its local environment, rather than a reference state. In addition, the definition of CAPE assumes that the parcel moves upwards and is positively buoyant at some lifted height, whereas APE density can be computed for parcels of any buoyancy.

If the local APE is integrated over a closed domain, and the Lorenzian reference state is used, the result will be identical to the Lorenz APE for that domain. The flexibility to use an alternative reference state is a particular advantage of the local theory for the moist atmosphere, where the Lorenz reference state is difficult to obtain, and the local definition means that budgets of APE density can be constructed to investigate local energy production and conversion. Local APE theory was recently generalised for a compressible multi-component fluid (Tailleux 2018), so it is now possible to apply the theory to the moist atmosphere to investigate the local APE budget of a numerically simulated TC. Further relevant details of local APE theory will be elucidated in Section 3.

Many energetic studies of TCs, both observational (Palmén and Jordan 1955; Palmén and Riehl 1957) and numerical (Kurihara 1975; Tuleya and Kurihara 1975; Hogsett and Zhang 2009), have

considered an energy pathway in which TPE is treated as the source of kinetic energy. Surface moisture fluxes increase the latent energy of low-level parcels as they flow in towards the centre of the TC (Kleinschmidt 1951; Emanuel 1986); as these parcels converge and rise in the eyewall, condensation occurs and releases latent heat, which converts this latent energy into TPE. TPE is then converted to kinetic energy via work produced by flow down the resulting radial pressure gradient.

Whilst this view of the energy transfers is not incorrect, it may not be the most useful one for understanding how diabatic processes lead to the generation of kinetic energy. Lorenz (1955) identified that the majority of TPE ($\approx 90\%$) is not available for reversible conversion into kinetic energy, and so when latent heat release generates TPE, only a small fraction of this should be expected to feed through into kinetic energy. Large amounts of TPE are exported in the upper level outflow (Palmén and Jordan 1955; Palmén and Riehl 1957; Hogsett and Zhang 2009), without contributing to the development of the TC in terms of kinetic energy.

If we do not expect the majority of TPE to be converted into KE, then it seems a poor choice to view as the reservoir of energy from which the TC extracts its KE. The ultimate intensification of the TC depends not just on the amount of TPE present, but on the efficiency with which this TPE can be converted to KE, i.e. how much of it is APE. Therefore, if the generation of kinetic energy in a TC is to be directly attributed to the effects of particular diabatic processes, it may be preferable to consider APE, rather than TPE, as the form of potential energy from which kinetic energy arises.

When considering TPE, the system efficiency of the TC is commonly measured by the ratio of latent heat release to kinetic energy generation. This will henceforth be referred to as the *TPE efficiency*. The TPE efficiency of a TC is very low—typically 2–3% (Palmén and Jordan 1955; Palmén and Riehl 1957; Hogsett and Zhang 2009)—and is difficult to calculate analytically. It has only been calculated analytically for very idealised dry vortices, using a constant heat forcing to approximate the effect of latent heat release (Schubert and Hack 1982; Hack and Schubert 1986). This makes it difficult to cleanly link diabatic processes to the TC's ultimate development; even if it is possible to budget the diabatic processes that contribute to a source of TPE, this source will mostly not lead to kinetic energy generation, and it is not easy to predict the efficiency with which it does.

In local moist APE theory, surface fluxes generate APE directly rather than via latent energy, because moist APE theory treats latent heat release as an internal parcel process rather than an external energy source. Any diabatic process can produce or dissipate APE, and the TC then intensifies as APE is converted into kinetic energy by buoyancy fluxes (Tailleux 2018). Each moist air parcel has its own APE production efficiencies, which govern how much APE density increases for a given change in entropy or total moisture content. These efficiencies will be fully defined in Section 3. The moist APE efficiencies are simpler to compute than TPE efficiency; this paper will demonstrate their computation for the axisymmetric model of Rotunno and Emanuel (1987). This means that spatially- and temporally-varying efficiencies can be computed in a model with interactive surface fluxes and convection, rather than requiring an unrealistic constant heat forcing. Since surface fluxes are expected to be a key source of APE, a moist APE-based diagnostic is also more likely to be able to incorporate the effects of boundary layer physics in future studies.

Another particularly useful theory, which is linked to the concept of efficiency in a TC, is that of potential intensity (PI). PI theory uses information about the thermodynamic environment of a TC to predict the maximum wind speed it can attain (its PI). The secondary circulation of a TC can be idealised as a reversible Carnot heat engine working between the boundary layer and the outflow; the *Carnot efficiency* of such an engine is

$$\eta = \frac{T_b - T_{\text{out}}}{T_b}, \tag{1}$$

where T_b is the temperature at the top of the boundary layer and T_{out} is the outflow temperature. The maximum wind speed at the top of the boundary layer v_b can then be derived as

$$v_b^2 = \frac{C_k}{C_D}\eta\,(k^* - k)\,, \tag{2}$$

where C_k and C_D are the surface exchange coefficients for enthalpy and momentum respectively, $k = c_p T + Lq$ is the moist enthalpy evaluated at the top of the mixed layer, and the saturation enthalpy k^* is evaluated at the sea surface temperature T_s (Emanuel 1988). A similar expression for PI can be derived without considering a Carnot engine, but by assuming gradient wind balance and saturated reversible thermodynamics above the boundary layer (Emanuel 1986). Recent work by Rousseau-Rizzi and Emanuel (2019) also showed that by considering two infinitesimally separated Carnot

cycles, it is possible to derive a PI for the surface winds without requiring the entire secondary circulation to approximate a Carnot heat engine: only the circulation in the eyewall needs to do so.

Although PI can be derived from an argument based on the maximum efficiency of a TC, there is not an obvious link between this Carnot efficiency and the TPE efficiency discussed above. The Carnot efficiency has a typical value of $\frac{1}{3}$, whereas the maximum TPE efficiency does not exceed 10‰ (this also applies to the efficiency of dry APE production; see Edmon Jr and Vincent (1979) for calculations). This may be linked to the fact that TPE and dry APE efficiencies treat latent heat release as their energy source, whereas in the Carnot engine framework the energy source is clearly surface enthalpy fluxes—as in moist APE theory. Many studies dealing with the Carnot cycle viewpoint of TCs refer to the mechanical energy output of the heat engine as the "available energy" (Emanuel 1987, 1997, 2003; Shen 2004). However, this energy is based on an entropy budget around a closed cycle and is therefore fundamentally different to the moist APE described here, which concerns the work done by buoyancy forces as air parcels move to a level of neutral buoyancy. Section 4a will explore the link between local moist APE theory and potential intensity.

While several studies have described APE as the source of energy for a TC (e.g. Anthes and Johnson 1968; Tang and Emanuel 2012; Wong et al. 2016), the difficulty of constructing a closed APE budget for a moist atmosphere has prevented a thorough analysis of the processes affecting moist APE in a TC. Since moist processes are of great importance in a TC, it is unsatisfactory to use a definition of APE based on the dry potential temperature, as was done by Anthes and Johnson (1968) and Nolan et al. (2007); this cannot take into account the full effects of moisture and its coupling with convection.

Tang and Emanuel (2012) used a local form of moist APE theory to explain how the ventilation of colder, drier air into a TC decreases its intensity: entropy mixing above the boundary layer destroys APE that could otherwise have been converted into kinetic energy. This work used an axisymmetric numerical model, and took the sounding used to initialise the model as the reference state. Tang and Emanuel (2012) did not derive a full budget of local APE for a multi-component fluid as in Tailleux (2018), but nonetheless their use of an LNB to compute parcels' reference properties yields a similar form for the efficiency of APE production to the full theory. This was an important demonstration of the physical insight that can be obtained by using moist APE theory, and using the initial model state as the reference state seems reasonable and minimises computational

expense. However, the work did not explore a full budget for the APE; for example, it is not known how much APE is stored in the TC or how much is converted to kinetic energy. Wong et al. (2016) also used moist APE to atudy an axisymmetric TC model, investigating which sorting algorithm yielded the most suitable reference state for studying intensification. However, the resulting APE production did not match kinetic energy generation in either of the tested reference states, and again a closed budget of APE was not computed.

In Section 2, we describe the axisymmetric TC model of Rotunno and Emanuel (1987) for which our local APE budget has been constructed. We highlight the key features of the model that informed the method of budget construction, such as the reference state and conserved variables. Section 3 then outlines the construction of the budget itself, and notes a discontinuous structure to the APE density that has not previously been described by local APE theory. This discontinuous character is an obstacle to physical interpretation of the APE budget for the TC, but demonstrates the benefit of constructing a complete, closed budget for a simple example case for providing insight into the fundamentals of local APE theory. In Section 4, we present the results of the APE budget. Further discussion, in particular how such a budget could be applied to a less idealised model, follows in Section 5.

2. Axisymmetric model

The axisymmetric tropical cyclone model of Rotunno and Emanuel (1987) (hereafter RE87) is a non-hydrostatic model designed to study the prototypical TC intensification problem, in which an existing vortex intensifies over a warm sea surface with no disturbance by a synoptic environment. More advanced axisymmetric TC models, such as CM1 (Bryan and Rotunno 2009), are available; the RE87 model lacks features such as a boundary layer scheme or dissipative heating. However, the construction of a local APE budget for a moist atmosphere is a complex procedure and so the simpler RE87 model is preferred in order to facilitate the development of a closed budget that accounts for the diabatic generation of APE by all modelled processes. The version of the model used here incorporates the modifications of Craig (1995, 1996), which introduce ice-phase microphysics and a closed radial boundary. Henceforth, this modified version of the RE87 model will be referred to as “the axisymmetric model", or simply “the model".

The axisymmetric model solves the compressible equations for nine prognostic variables: the radial, azimuthal and vertical components of velocity, u, v and w; the perturbation of the Exner pressure from the initial environmental sounding, $\pi = \Pi - \overline{\Pi}$; the potential temperature, θ; and the mixing ratios of water vapour r_v, cloud liquid water r_l, liquid precipitation r_p, and ice r_i. Section 2a will describe the setup of the model domain and the initial conditions for these equations. Section 2b will derive the model's kinetic energy budget from the three components of the momentum equation, and the available elastic energy budget from the equation for π. Section 2c will use the equations for the thermodynamic variables to identify the conserved variables required to construct the APE budget in Section 3.

a. Model setup

The model is run at a radial resolution of $r = 2.5$ km and a vertical resolution of $z = 625$ m. This resolution is high enough to permit convection, so that the conversion of available potential energy into kinetic energy via convection can be studied without the need to consider a convective parameterisation. The resolution is not increased any further due to the high computational expense of APE diagnostics. Model output is analysed at hourly intervals.

The domain measures 22.5 km in the vertical direction, with a further 5 km of sponge layer, in which the three components of velocity are damped to absorb gravity waves, so that these do not reflect from the upper boundary. The domain extends 3150 km in the radial direction, and the no-flux outer boundary condition of Craig (1996) is used. An outer sponge layer of 900 km was required to absorb radially-propagating gravity waves. Using these parameters, the intensification of the TC is not found to be sensitive to the radial extent of the domain. The domain is assumed to be an f-plane with Coriolis parameter $f = 6.14 \times 10^{-5}$ rad s^{-1}, corresponding to a latitude of approximately 25°N.

The model's initial conditions are determined by the sea surface temperature, which remains constant throughout the run, the far-field environmental sounding, and the azimuthal wind profile of the vortex. The results shown in this paper were obtained using an SST of 30.3°C and the Jordan mean hurricane-season sounding for the West Indies (Jordan 1958). The effects of changing the SST and environmental sounding will be discussed briefly in Section 5.

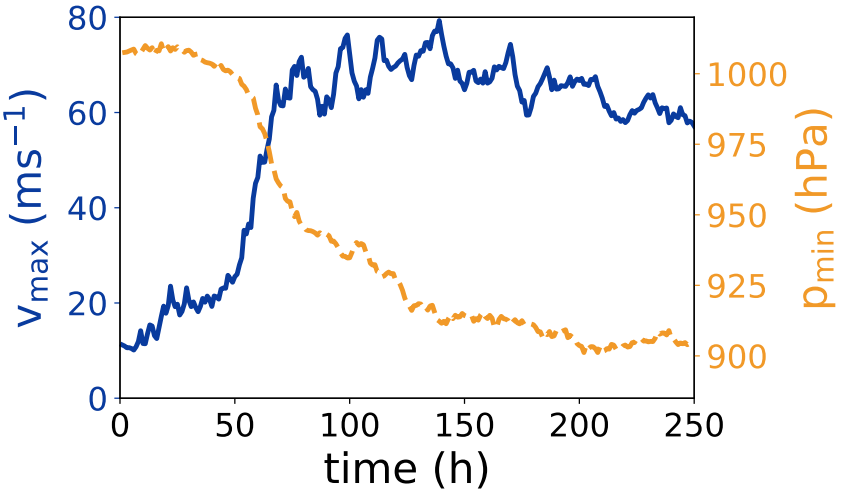

FIG. 1: Intensity of the TC produced by the axisymmetric model, in terms of maximum azimuthal wind speed (blue solid line) and minimum surface pressure (orange dashed line).

The azimuthal wind of the initial vortex is prescribed as in Emanuel and Rotunno (1989), with a maximum wind speed $v_{max} = 12$ m s^{-1} occurring at radius $r_{max} = 75$ km. The initial thermodynamic fields are adjusted to achieve thermal wind balance with the prescribed vortex before simulation of the cyclone intensification begins. The intensity of the simulated TC in terms of both maximum azimuthal wind speed v_{max} and minimum surface pressure p_{min} is shown in Figure 1. The initial stages of intensification, from 5 to 40 h, are relatively slow; this is followed by a period of rapid intensification (RI) from 40 to 75 h; v_{max} increases by 49.7 m s^{-1} over this 35 h, easily exceeding the 15 m s^{-1} increase in 24 h by which RI is usually defined (Kaplan et al. 2010; Lee et al. 2016). This RI period is also marked by a fast deepening of the central pressure. The maximum value of v_{max} is 79.3 m s^{-1}, attained at 139 h. There is then an overall decreasing trend in v_{max} from 139 h to 250 h.. The central pressure decreases until it becomes approximately steady at approximately 200 h, with an average value of 904.4 hPa over the final 50 h of the simulation.

b. Model energetics

The model's momentum equations can be written as:

$$\frac{D\vec{v}}{Dt} = -\left(f + \frac{v}{r}\right)\vec{v}\times\widehat{\vec{z}} - c_p\overline{\theta_v}\nabla\pi + b\widehat{\vec{z}} + \vec{D}, \tag{3}$$

where overbars denote variables in the initial sounding; these variables vary in the vertical direction only. The velocity has components $\vec{v} = (u, v, w)$, and the unit vector in the vertical direction is denoted by $\widehat{\vec{z}}$. The Lagrangian derivative in axisymmetric cylindrical coordinates is $\frac{D}{Dt} = \frac{\partial}{\partial t} + u\frac{\partial}{\partial r} + w\frac{\partial}{\partial z}$, and $\theta_v = \theta(1 + 0.61 r_v)$ is the virtual potential temperature. The specific heat capacity at constant pressure of dry air is $c_p = 1004.5$ J kg-1 K^{-1}. The term $\vec{D} = (D_u, D_v, D_w)$ parameterises subgrid turbulence based on a Richardson number-dependent eddy viscosity. The scale of the mixing is set by horizontal and vertical mixing lengths. These are set to the model's default values for the chosen resolution, which are 500 m and 200 m respectively. This term also includes the effects of surface friction on the momentum, as documented in RE87. The buoyancy b is defined by

$$b = g\left\{\frac{\theta - \overline{\theta}}{\overline{\theta}} + 0.61\,(r_v - \overline{r}_v) - r_l - r_p - r_i\right\}. \tag{4}$$

Our required equation for the specific kinetic energy $e_k = \frac{\vec{v}^2}{2}$ is obtained by taking the dot product of $\overline{\rho}\vec{v}$ with (3):

$$\overline{\rho}\frac{De_k}{Dt} = -\overline{\rho} c_p \overline{\theta_v}\vec{v} \cdot \nabla\pi + \overline{\rho} b w + \overline{\rho}\vec{v} \cdot \vec{D}, \tag{5}$$

which we can write in flux form as

$$\frac{\partial(\overline{\rho} e_k)}{\partial t} = -\nabla \cdot (\overline{\rho} e_k \vec{v}) + e_k \nabla \cdot (\overline{\rho}\vec{v}) - \overline{\rho} c_p \overline{\theta_v}\vec{v} \cdot \nabla\pi + \overline{\rho} b w + \overline{\rho}\vec{v} \cdot \vec{D}. \tag{6}$$

The second term on the RHS of (6) results from the fact that the axisymmetric model does not enforce the anelastic continuity equation $\nabla \cdot (\overline{\rho}\vec{v}) = 0$; we will therefore refer to it as the *elastic mass divergence term*, similar to the terminology used by Xue and Lin (2001). In practice, this term is very small in all the budgets presented in this paper.

We next derive the equation for the model's available elastic energy, e_e. For small pressure perturbations π, the elastic energy is approximately

$$e_e = \frac{c_p^2 \overline{\theta_v}^2}{\overline{c}^2}\frac{\pi^2}{2} \tag{7}$$

(e.g. Bannon 2003; Peng et al. 2015; Tailleux 2018). The speed of sound in the initial model state is defined by $\overline{c}^2 = \frac{c_p R_d \overline{\Pi}\,\overline{\theta_v}}{c_v}$, where $c_v = 717.5$ J kg^{-1} K^{-1} is the specific heat capacity at constant volume of dry air. The model's equation for the time tendency of π is

$$\frac{\partial \pi}{\partial t} = -\frac{\overline{c}^2}{c_p \overline{\rho}\,\overline{\theta_v}^2} \nabla \cdot \left(\overline{\rho}\overline{\theta_v}\vec{v} \right) + \frac{\overline{c}^2}{c_p \overline{\theta_v}^2} \frac{D\theta_v}{Dt}, \tag{8}$$

with the divergence operator in axisymmetric cylindrical coordinates given by $\nabla \cdot \vec{\psi} = \frac{1}{r}\frac{\partial (r\psi_r)}{\partial r} + \frac{\partial \psi_z}{\partial z}$ for a vector $\vec{\psi} = (\psi_r, \psi_\theta, \psi_z)$. Equation (8) is an approximation to the mass conservation equation derived by Klemp and Wilhelmson (1978). The term proportional to $\frac{D\theta_v}{Dt}$ appears in the full derivation, but was neglected in the original RE87 model. It has been re-included here to prevent the strong diabatic heating in the eyewall leading to a large mass sink, as documented by Tang (2010).

We can multiply Equation (8) by $\overline{\rho}\frac{c_p^2 \overline{\theta_v}^2}{\overline{c}^2}\pi$ to obtain the available elastic energy budget

$$\begin{aligned} \frac{\partial \left(\overline{\rho} e_e \right)}{\partial t} &= -c_p \pi \nabla \cdot \left(\overline{\rho}\overline{\theta_v}\vec{v} \right) + \overline{\rho} c_p \pi \frac{D\theta_v}{Dt} \\ &= -\nabla \cdot \left(\overline{\rho} c_p \overline{\theta_v} \pi \vec{v} \right) + \overline{\rho} c_p \overline{\theta_v} \vec{v} \cdot \nabla \pi + \overline{\rho} c_p \pi \frac{D\theta_v}{Dt}, \end{aligned} \tag{9}$$

where the divergence term has been rearranged to establish the link between the available elastic and kinetic energies via the reappearance of the term $\overline{\rho} c_p \overline{\theta_v} c_p \vec{v} \cdot \nabla \pi$. The three terms of the budget on the RHS are respectively: the pressure work performed on the domain boundaries, the conversion between kinetic energy and available elastic energy, and the change in available elastic energy due to the mass correction associated with changes in θ_v.

The budget for the sum of the kinetic and elastic energies is then

$$\frac{\partial \left[\overline{\rho} \left(e_k + e_e \right) \right]}{\partial t} = -\nabla \cdot \left[\overline{\rho} \left(e_k + c_p \overline{\theta_v} \pi \right) \vec{v} \right] + e_k \nabla \cdot \left(\overline{\rho}\vec{v} \right) + \overline{\rho} c_p \pi \frac{D\theta_v}{Dt} + \overline{\rho}\vec{v} \cdot \vec{D} + \overline{\rho} b w. \tag{10}$$

In order, the terms on the RHS of this equation are: the flux of mechanical energy density, as described by Gill (1982), Smith et al. (2018); small sources or sinks of kinetic energy due to the elastic mass divergence term; changes in available elastic energy due to the heating correction term in the pressure equation; the frictional dissipation of kinetic energy; and the vertical buoyancy flux,

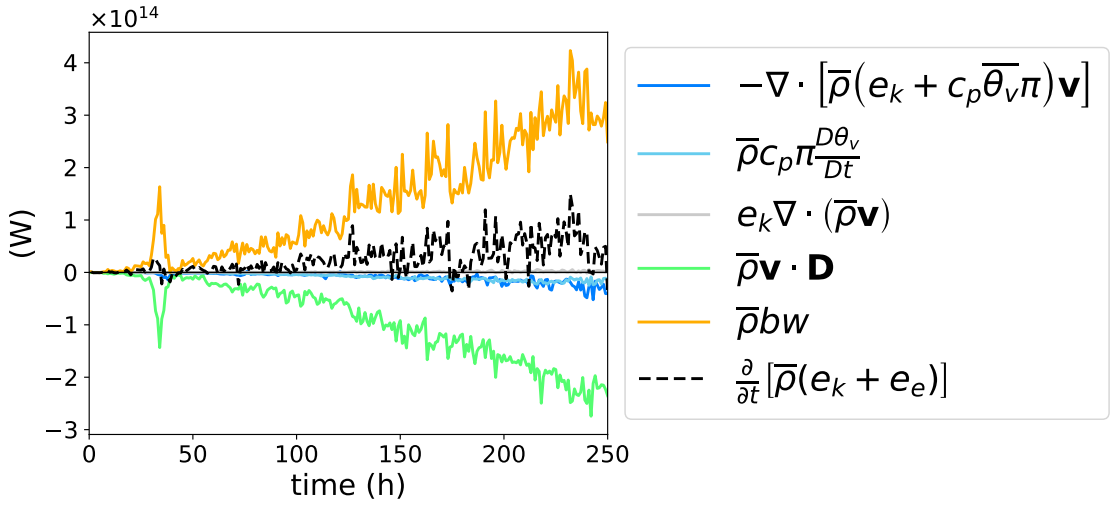

FIG. 2: Budget of kinetic plus available elastic energy according to Equation (10), integrated over the axisymmetric model domain. The horizontal black line marks 0 W.

which is the conversion between APE and kinetic energy. This final term will therefore appear with the opposite sign in the APE budget in Section 3, where we will investigate how it is linked to the generation of APE by diabatic processes.

Figure 2 shows the budget of kinetic and elastic energy integrated over the whole model domain (excluding sponge layers). The main energy balance is between the conversion of APE into kinetic energy and the frictional dissipation of kinetic energy, which occurs mostly at the sea surface. The storage of azimuthal kinetic energy and available elastic energy as the cyclone develops result in a positive total tendency.

It is important to recognise that this interpretation of the energy budget is not at odds with the traditional view that kinetic energy is generated by the acceleration of inflowing parcels by the radial pressure gradient (e.g. Anthes 1974). This conversion is implicit within the total kinetic + elastic energy budget. The vertical kinetic energy generated by the conversion of APE is very quickly converted to elastic energy via the vertical pressure gradient, resulting in the total vertical kinetic energy in the model being much smaller than the horizontal kinetic energy. It is therefore still the work of the radial pressure gradient that generates most of the kinetic energy in the modelled TC.

c. Conserved variables

The model's conserved variables are of particular interest to the construction of an APE budget, as we will need to make a choice of conserved variables when lifting parcels reversibly and adiabatically to their reference heights. The original axisymmetric model was noted by Rotunno and Emanuel (1987) to approximately conserve equivalent potential temperature

$$\theta_e = \theta \exp\left(\frac{L_v r_v}{c_p T}\right), \tag{11}$$

in near-saturation conditions, where L_v is the latent heat of vaporisation of water. As before, the D_j terms are subgrid turbulence parameterisations (which include surface fluxes of θ and r_v). R is a radiative cooling tendency, for which we use the simple Newtonian cooling of Rotunno and Emanuel (1987), with a limit of 2 K day^{-1}, as recommended by Tang and Emanuel (2012).

The approximate material derivative of θ_e is

$$\frac{D\theta_e}{Dt} \approx \frac{D\theta}{Dt} + \frac{L_v}{c_p \Pi}\frac{Dr_v}{Dt} = D_\theta + \frac{L_v}{c_p \Pi} D_{r_v} + R, \tag{12}$$

so that θ_e is conserved by all processes other than radiative cooling and the subgrid contributions to θ and r_v, when variation in Π is neglected.

The modifications by Craig (1995) add rainwater and ice variables to the model. We extend θ_e to include these with

$$\theta_{ei} = \theta \exp\left(\frac{L_s r_v}{c_p T}\right) \exp\left[\frac{L_f \left(r_l + r_p\right)}{c_p T}\right], \tag{13}$$

Here, L_s is the latent heat of sublimation and L_f is the latent heat of fusion. This choice of θ_{ei} as a modified potential temperature is based on the definition of Pauluis (2016), but neglects variations in c_p and T since these are not accounted for in the model. Again neglecting variations in Π, the material derivative of θ_{ei} is

$$\begin{aligned}\frac{D\theta_{ei}}{Dt} &\approx \frac{D\theta}{Dt} + \frac{L_s}{c_p \Pi}\frac{Dr_v}{Dt} + \frac{L_f}{c_p \Pi}\frac{D\left(r_l + r_p\right)}{Dt} \\ &= D_\theta + \frac{L_s}{c_p \Pi} D_{r_v} + \frac{L_f}{c_p \Pi}\left(D_{r_l} + D_{r_p} + P_{r_p}\right) + R,\end{aligned} \tag{14}$$

where P_{r_p} is the fallout of liquid precipitation. Whilst Equation (11) defined a θ_e that is approximately conserved by condensation and evaporation of cloud liquid water, θ_{ei} is also approximately conserved by the freezing, melting and sublimation processes included as part of the modified microphysics.

The neglect of variation in Π in Equation (14) poses an obstacle for the APE budget. If the APE density e_a is computed for moist air parcels based on the definition of θ_{ei} in Equation (13), then changes in e_a will result from changes in θ_{ei} according to the material derivative

$$\frac{D\theta_{ei}}{Dt} = \frac{D\theta}{Dt} + \frac{L_s}{c_p\Pi}\frac{Dr_v}{Dt} + \frac{L_f}{c_p\Pi}\frac{D\left(r_l+r_p\right)}{Dt} - \frac{L_s r_v + L_f\left(r_l+r_p\right)}{c_p\Pi^2}\frac{D\Pi}{Dt}. \tag{15}$$

The term proportional to $\frac{D\Pi}{Dt}$ will change θ_{ei} and therefore appear to contribute to the diabatic production/dissipation of e_a, but it is not associated with the production of APE due to any diabatic process in Equation (14). To solve this problem, the density-weighted average of Π throughout the domain (over all time steps) is computed; this will be denoted by $\widetilde{\Pi}$. When computing θ_{ei} for use in the APE budget, it is approximated to

$$\theta_{e_i} \approx \theta + \frac{L_s r_v}{c_p\widetilde{\Pi}} + \frac{L_f\left(r_l+r_p\right)}{c_p\widetilde{\Pi}}, \tag{16}$$

and wherever Π appears in the definitions of the APE production coefficients it is replaced with $\widetilde{\Pi}$. This results in a production of APE by changes in θ_{e_i} that is approximately equal to the production computed directly from the surface fluxes, subgrid mixing and precipitation fallout, when integrated regionally.

A second approximately conserved variable is given by the total mixing ratio

$$r_t = r_v + r_l + r_p + r_i, \tag{17}$$

$$\frac{Dr_t}{Dt} = \sum_j D_{r_j} + P_{r_p} + P_{r_i}, \tag{18}$$

with $j = v, l, p, i$, where P_{r_i} is the fallout of ice-phase precipitation. The variables (θ_{ei}, r_t) are approximately conserved by all modelled processes other than radiative cooling, the fallout of precipitation (both liquid and ice), surface fluxes, and subgrid turbulence and frictional dissipation.

Next, we use the findings of this section to design an appropriate budget of APE density for the axisymmetric model.

3. Available Potential Energy budget

The local form of APE theory was originally developed by Andrews (1981) and Holliday and McIntyre (1981) and was recently generalised for a multicomponent compressible stratified fluid by Tailleux (2018). For each fluid parcel, APE density is defined as the energy released when the parcel moves reversibly and adiabatically to its nearest level of neutral buoyancy (LNB) with respect to a reference state, which is a notional resting atmospheric state. The APE thus gives the total potential energy that is available for reversible conversions into kinetic energy.

As was discussed in Section 2, the axisymmetric model equations are defined with respect to an initial sounding. We therefore take this initial sounding as our reference state, since it represents the undisturbed environment in which the TC intensifies. The reference state is in hydrostatic equilibrium:

$$\frac{\mathrm{d}\overline{p}}{\mathrm{d}z} = -\frac{g}{\overline{\alpha}}, \tag{19}$$

where α is specific volume. For each parcel, the reference height z_r is defined using the equation for the parcel's LNB when it is lifted reversibly and adiabatically,

$$\alpha(\theta_{ei}, r_t, \overline{p}\,(z_r)) = \overline{\alpha}\,(z_r)\,. \tag{20}$$

Here, we have used the equivalent potential temperature and total mixing ratio to define reversible adiabatic lifting, since these were identified to be approximately conserved variables in Section 2.

If a parcel is positively buoyant at its position z, its first LNB above z is selected as z_r; if no such LNB exists then the height at the top of the domain is used. If the parcel is negatively buoyant at z then z_r is chosen as the first LNB below z, or the bottom of the domain if this LNB does not exist. Defining the parcel's buoyancy relative to the reference state as

$$b\,(\theta_{ei}, r_t, z) = g\frac{\alpha\,[\theta_{ei}, r_t, \overline{p}\,(z)] - \overline{\alpha}\,(z)}{\overline{\alpha}\,(z)}, \tag{21}$$

the parcel's APE density is

$$e_a = \int_z^{z_r} b\left(\theta_{ei}, r_t, z'\right) dz'. \tag{22}$$

The evolution equation for e_a is then derived (see Tailleux (2013) for more details) as

$$\begin{aligned}\frac{De_a}{Dt} = &\underbrace{\int_z^{z_r} \frac{\partial b}{\partial \theta_{ei}}\left(\theta_{ei}, r_t, z'\right) dz'}_{G_{\theta_{ei}}} \frac{D\theta_{ei}}{Dt} \\ &+ \underbrace{\int_z^{z_r} \frac{\partial b}{\partial r_t}\left(\theta_{ei}, r_t, z'\right) dz'}_{G_{r_t}} \frac{Dr_t}{Dt} \\ &- bw + b(z_r)\frac{Dz_r}{Dt},\end{aligned} \tag{23}$$

where $G_{\theta_{ei}}$ and G_{r_t} are APE production coefficients, which govern the amount of e_a produced by a given change in θ_{ei} and r_t respectively. These derivatives are sometimes referred to as thermodynamic efficiencies (Tailleux 2013), but here the terminology *efficiency* is reserved for the scaled forms of the coefficients that will be defined later in this section, since these take values between -1 and 1 and can therefore be more easily compared with other definitions of efficiency. The term $-bw$ is the conversion between APE density and KE via vertical buoyancy fluxes. The derivation of the term proportional to $\frac{Dz_r}{Dt}$ assumes that z_r varies continuously, in which case the term vanishes since $b\left(z_r\right) = 0$. However, more consideration is required when z_r varies discontinuously, as discussed later in this section.

The forms of the APE production coefficients can be found by using the generalised theory of Tailleux (2018) and rearranging for our particular choice of conserved variables. Defining the subscripts h, r by $f_h = f\left(\theta_{ei}, r_t, \overline{p}\left(z\right)\right), f_r = f\left(\theta_{ei}, r_t, \overline{p}\left(z_r\right)\right)$ for any thermodynamic variable f, the efficiencies are

$$G_{\theta_{ei}} = c_p \frac{T_h - T_r}{\theta_{ei}}, \tag{24}$$

$$G_{r_t} = \frac{1}{\left(1+r_t\right)^2}\left[\mu_h - \mu_r - \left(T_h - T_r\right)\frac{\partial \mu}{\partial T}\right], \tag{25}$$

where μ is chemical potential. Here, the specific heat capacity for moist air has been defined as $c_p = \frac{c_{pd} + r_t c_i}{1+r_t}$.

In order to obtain a closed budget of APE density for the axisymmetric model, it is necessary to discretise $e_a, G_{\theta_{ei}}$ and G_{r_t} on the model grid, and account for approximations inherent in the model's definitions of thermodynamic variables and buoyancy. Full details of the discretisations and approximations used to compute these quantities are included in Appendix A.

We define the *APE production efficiencies* by scaling the APE production coefficients so that they approximate the APE produced for a given change in enthalpy. If the effect of the latent heat of fusion is included in the definition of enthalpy, a change $d\theta_{ei} = d\theta + \frac{L_s}{c_p \Pi} dr_v$ corresponds to an enthalpy change $dk = c_p dT + L_s dr_v \approx c_p \Pi d\theta + L_s dr_v = c_p \Pi d\theta_{ei}$. Assuming no changes in r_l, r_p or r_i for simplicity, the change in r_t is $dr_t = dr_v$, which is equivalent to an enthalpy change $dk = L_s dr_v$. The APE production efficiencies with respect to θ_{ei} and r_t are therefore defined as

$$\varepsilon_{\theta_{ei}} = \frac{G_{\theta_{ei}}}{c_p \Pi}, \tag{26}$$

$$\varepsilon_{r_t} = \frac{G_{r_t}}{L_s}, \tag{27}$$

which provide efficiency values between -1 and 1. The material derivative of APE (Equation (23)) can be rewritten in terms of the production efficiencies as

$$\frac{De_a}{Dt} = \varepsilon_{\theta_{ei}} c_p \Pi \frac{D\theta_{ei}}{Dt} + \varepsilon_{r_t} L_s \frac{Dr_t}{Dt} - b\,(z)\, w + b(z_r) \frac{Dz_r}{Dt}. \tag{28}$$

The final term on the RHS of (28) has been taken to be zero in previous works, since $b\,(z_r) = 0$ by the definition of the reference height (Tailleux 2013). However, to obtain this form of the term from the Lagrangian derivative of Equation (22), it is necessary to assume that z_r is a continuous function of space and time, which need not be the case. Recognising that discontinuous transitions in z_r and hence e_a can occur is crucial to closing the local APE budget in some scenarios. Here we provide one example to illustrate how these transitions may occur.

Using the Jordan mean hurricane season sounding as a reference profile, we take an example parcel at $z = 100$m with $\theta_e = 340\,\mathrm{K}$, $r_t = 0.014\,\mathrm{kgkg}^{-1}$. The parcel is positively buoyant with respect to the reference profile and so $z_r > z$. Figure 3a shows the parcel's temperature and liquid water mixing ratio as it is lifted reversibly and adiabatically along the reference pressure profile $\overline{p}\,(z)$ (for

this illustration, freezing has not been included). From this we can see that the parcel becomes saturated just below a height of 2 km.

The parcel's reference height z_r is then the lowest height z at which $b(z) = 0$. The lifted buoyancy profile is shown by the solid line in Figure 3b, with the dashed line indicating where $b = 0$. The parcel reaches neutral buoyancy shortly before it saturates. In this case $z_r = 1.25\,\mathrm{km}$ (indicated by the lower green star). If the parcel were heated so that $\theta_e = 341\,\mathrm{K}$, while maintaining constant r_t, its new buoyancy profile would be the one shown by the dashed-dotted line. The parcel now remains positively buoyant around its saturation level, and attains a much higher LNB, $z_r = 13.2\,\mathrm{km}$ (indicated by the upper green star). At some temperature $340\,\mathrm{K} < \theta_e < 341\,\mathrm{K}$, z_r discontinuously transitions from 1.25 km to 13.2 km without taking on any value in between. Therefore, even if θ_e varies continuously in time and space, temporal discontinuities in z_r and hence e_a can occur. Spatial discontinuities in e_a are then also expected, as a result of the fact that one parcel may have accessed a higher LNB in this manner whilst a neighbouring parcel, despite having similar thermodynamic properties, has not.

The example presented above is analogous to the release of Convective Available Potential Energy, the main difference being that buoyancy is defined relative to the reference state rather than necessarily the local environment. At $\theta_e = 340\,\mathrm{K}$, z_r lies below the parcel's level of free convection (LFC); we can think of some APE being unavailable to the parcel due to the presence of convective inhibition (CIN). The perturbation of θ_e by 1 K is sufficient to allow the parcel to attain its LFC and hence rise to its LNB at 13.2 km, releasing APE in the same way that CAPE would be released.

The discontinuous behaviour of z_r is a signal that a reservoir of Background Potential Energy (BPE) has become APE (recall that BPE is the part of the total potential energy not available for reversible conversion to kinetic energy; TPE = APE + BPE). Similar behaviour can be seen in cases where the parcel's *in situ* buoyancy is close to zero, so that a small amount of heating or moistening may switch a parcel with marginally negative buoyancy and $z_r = 0\,\mathrm{m}$ to a positively buoyant parcel with z_r high in the troposphere (or vice versa).

However, since APE is defined relative to a non-local sounding in this case, the appearance of large amounts of APE has less physical significance than the release of CAPE. When CAPE is released, deep convection occurs as parcels move to their LNB. However, in the case of APE, a parcel could have z_r high in the troposphere when calculated relative to some far-field environmental

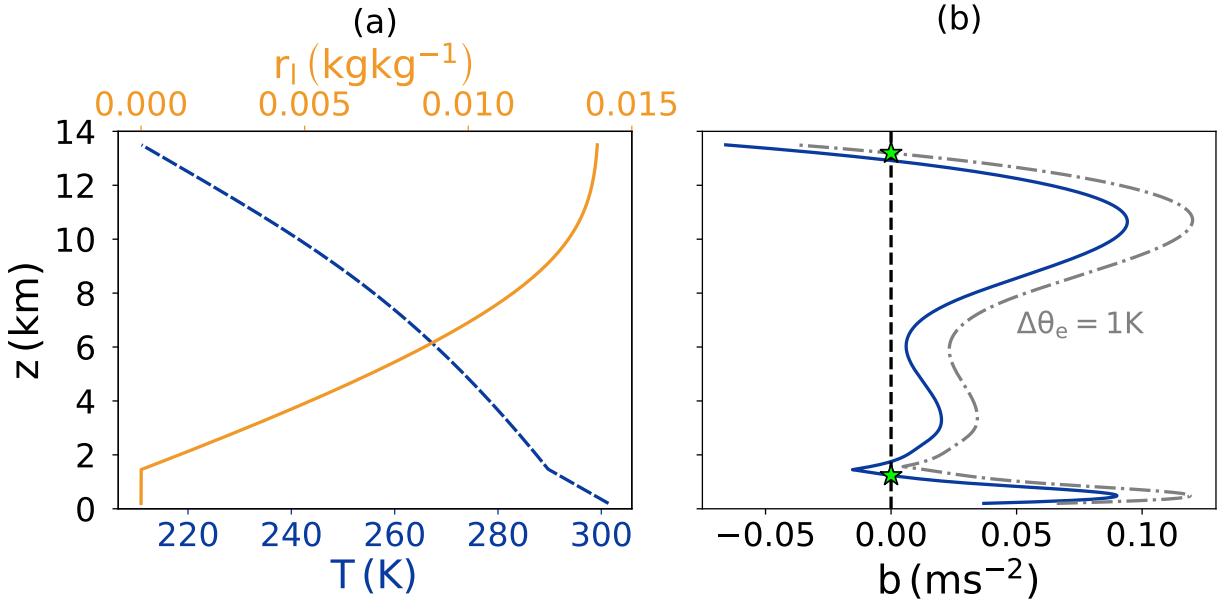

FIG. 3: Thermodynamic properties of a parcel with $\theta_e = 340\,\mathrm{K}, r_t = 0.014\,\mathrm{kg\,kg^{-1}}$ when lifted reversibly and adiabatically upwards from 200 m through the Jordan hurricane-season mean sounding (freezing not included). (a) Temperature (dashed blue line) and liquid water mixing ratio (solid orange line) as parcel is lifted. (b) Buoyancy relative to Jordan sounding during lifting (blue solid line). The grey dashed-dotted line shows the buoyancy profile when θ_e is perturbed by 1 K. The black dashed line indicates where $b = 0$ m s^{-2}. Green stars mark reference heights for the two parcels.

sounding, but not actually move upwards because it is not buoyant relative to its local environment. It is therefore important to bear in mind that a discontinuous increase in local APE need not be associated with any rapid change in vertical motion.

The discontinuous behaviour of z_r is not unique to the atmospheric context; the possibility of the existence of multiple LNBs has also been identified in the ocean (Saenz et al. 2015), which would enable discontinuous transitions of z_r in seawater parcels.

The discontinuity of z_r in time can be thought of as an instantaneous transfer of potential energy into APE from BPE. As z_r transitions, the partition between APE and BPE is suddenly altered. This view contrasts with previous interpretations of local APE budgets, in which transfer between APE and BPE occurs only through diabatic processes. Here, the transfer may occur adiabatically via changes in z_r (although the transition could be triggered by diabatic processes).

Some part of the BPE can be considered to be latent APE, meaning that it is not available for reversible conversion to kinetic energy, but it can become so without the need for diabatic processes.

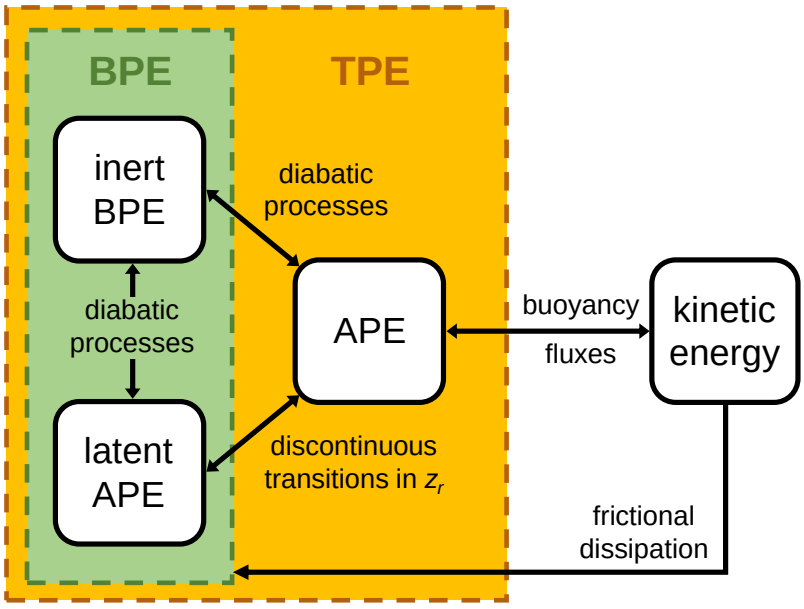

FIG. 4: Possible transfers between forms of potential energy and kinetic energy when z_r can exhibit discontinuity. External energy sources (e.g. surface fluxes) are not included.

In contrast, the rest of the BPE is inert, i.e. it will not become APE without diabatic processes altering the partition between BPE and APE. These forms of potential energy and the transfers between them are depicted in Figure 4. Discontinuous transitions may either convert latent APE to APE, as described above, or vice versa, if the transition moves the reference height closer to the parcel's actual position (for example, if the parcel illustrated in Figure 3 were cooled from 341 K to 340 K). Latent APE can be generated from inert BPE by diabatic processes in much the same way that APE is generated, but latent APE must undergo a transition to APE before it can be converted to kinetic energy.

In light of the possibility of such discontinuous behaviour in z_r, Eq. (23) should be reformulated as

$$\frac{De_a}{Dt} = \varepsilon_{\theta_{ei}} c_p \Pi \frac{D\theta_{ei}}{Dt} + \varepsilon_{r_t} L_s \frac{Dr_t}{Dt} - bw + \text{discontinuities}. \tag{29}$$

The formal mathematical representation of the discontinuity term would involve Dirac delta functions. However, it is difficult to work with delta functions on a discretised grid, because the discontinuous transitions will generally occur at some location between grid points. For this reason, in the APE budget the final term on the RHS of Equation (29) is diagnosed as a budget residual,

computed only for grid points that show variations in z_r consistent with discontinuous behaviour. The residual is computed for parcels that exhibit a change in z_r of greater than the vertical grid spacing Δz in a single time step. The residual is also computed if a grid point has either radially or vertically neighbouring points with a difference in z_r greater than $10\Delta z$ (a higher threshold is used than for the temporal discontinuity because there may be large variations in θ_{ei} and r_t between grid points, so some larger changes in z_r are to be expected).

When presenting results from the axisymmetric model, we mask out the contribution of temporal discontinuities to the APE budget, because otherwise these introduce high-magnitude noise to the budget and prevent analysis of the continuous evolution of APE due to diabatic processes. The conversion of APE to kinetic energy does not exhibit any apparent temporal discontinuities. Therefore, the continuous evolution appears to be more physically relevant to intensification. It is not possible to assess the overall effect that the temporal discontinuities have on the evolution of the total APE, because the model data is only output every hour, whereas discontinuities happen on a single 6 s time step, and may contribute very differently from one time step to the next. Such sparse sampling is not adequate to capture the overall effect of the discontinuities, but it would not be feasible to perform the APE budget on the large amount of data required to capture processes occurring on the scale of single time steps. Spatial discontinuities in APE density are included in the results.

With the issue of discontinuity addressed, it is now possible to compute the complete APE budget for the axisymmetric model. To ensure that no physically important effects are being hidden by the temporal discontinuity masking, the budget presented in Section 4 will be one in which temporal discontinuities vanish in the mature stage. Figures verifying the closure of the budgets presented in Section 4 are presented in Appendix B. The final form of the APE budget used is

$$\frac{\partial\left(\overline{\rho}e_a\right)}{\partial t} = -\nabla\cdot\left(\overline{\rho}e_a\vec{v}\right) + e_a\nabla\cdot\left(\overline{\rho}\vec{v}\right) + \overline{\rho}\varepsilon_{\theta_{ei}}c_p\Pi\frac{D\theta_{ei}}{Dt} + \overline{\rho}\varepsilon_{r_t}L_s\frac{Dr_t}{Dt} - \overline{\rho}bw + \text{discontinuities}, \quad (30)$$

where we have transformed Equation (29) into flux form using the fact that $\overline{\rho}$ is independent of time. The terms contributing to the time tendency of APE in a fixed volume are: the flux of APE through the volume boundaries; a source/sink of APE due to elastic mass divergence; the diabatic

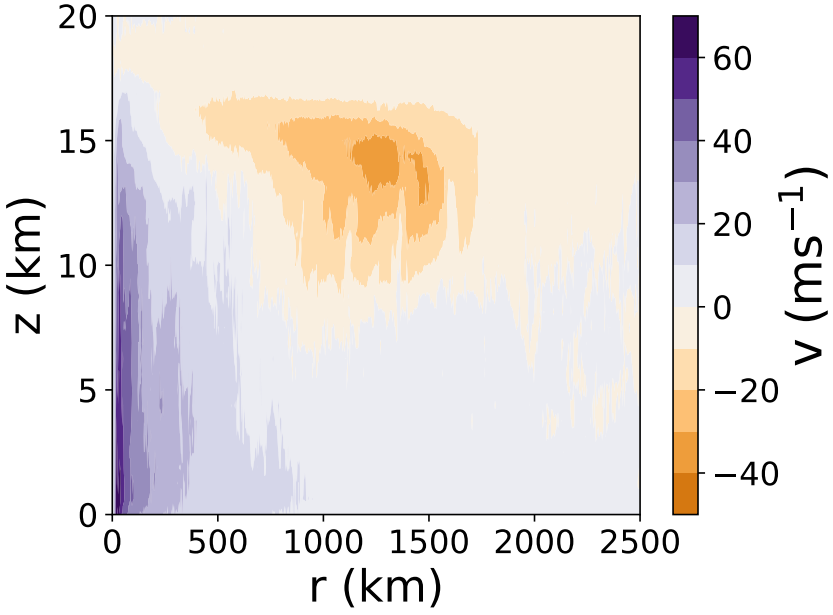

FIG. 5: Azimuthal wind v of the axisymmetric TC at 150 h. Coloured contour levels are spaced every 10 m s^{-1}. Purple shading corresponds to positive v (cyclonic flow), while orange shading corresponds to negative v (anticyclonic flow).

production/dissipation of APE, dependent on the APE production efficiencies $\varepsilon_{\theta_{ei}}$ and ε_{r_t}; the conversion between APE and vertical kinetic energy; and spatial discontinuities in APE.

4. Results

Before presenting the full APE budget, we first examine the APE density and production efficiencies. Figure 5 shows the azimuthal wind speed at 150 hours into the model run to provide context for the scale and structure of the TC; the APE density e_a at the same time is shown in Figure 6. The highest values of e_a occur near the cyclone centre and at the sea surface. The high APE density in the centre reflects the baroclinicity of the system; APE is stored in the warm core of the cyclone relative to the initial environment. This APE could be released if the vortex were to dissipate. The high APE at the surface seems likely to be a result of the production of APE by air-sea fluxes, which will be verified by further budget analysis later in this section.

Figures 7 shows the APE production efficiencies $\varepsilon_{\theta_{ei}}$ and ε_{r_t}, again at 150 hours. The two efficiencies are broadly similar in pattern and generally of opposite sign. The similar pattern results from the dependence of both efficiencies on the reference height z_r. Where $|z - z_r|$ is large,

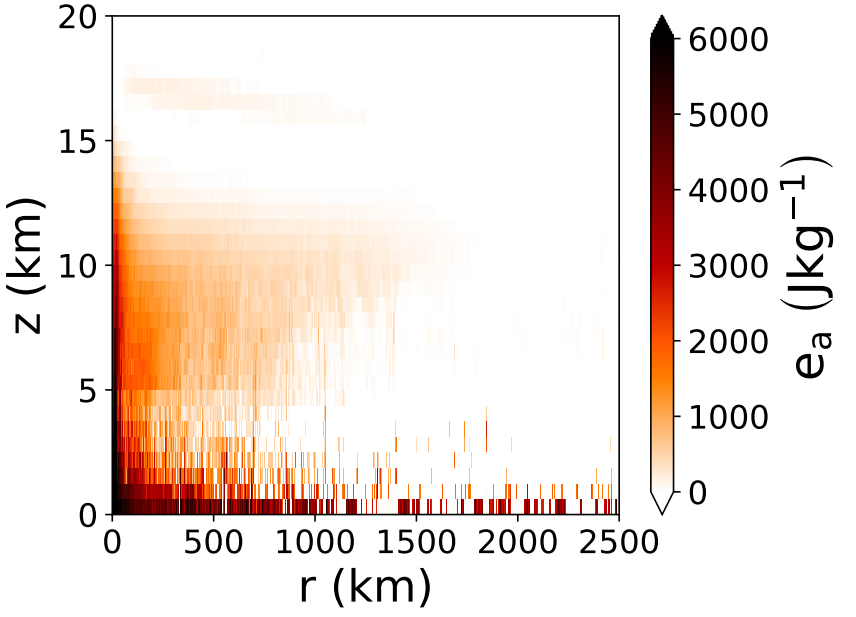

FIG. 6: APE density e_a in the axisymmetric TC 150 h into the simulation, computed using a discretised version of Equation (22).

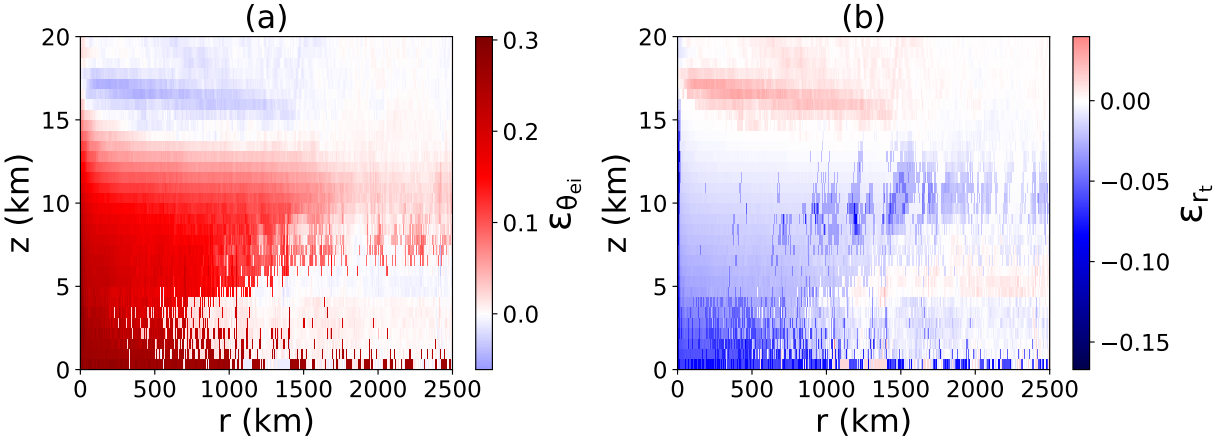

FIG. 7: APE production efficiencies at 150 h. Red parcels have positive efficiency, meaning that an increase in the relevant quantity (θ_{ei} for (a), r_t for (b)) will increase e_a. Blue parcels have negative efficiency, meaning that an increase in the quantity will decrease e_a.

the air parcel will have very different properties at its reference height versus its actual height, so $|T_h - T_r|$ and $|\mu_h - \mu_r|$ are both large. Hence the magnitudes of the efficiencies tend to covary.

Regions in which $\varepsilon_{\theta_{ei}}$ is positive are the regions in which air is positively buoyant and therefore $z_r > z$. An increase in θ_{ei} will further increase the buoyancy, leading to an increase in APE density.

We can therefore conclude that surface fluxes of θ_{ei} will generally produce APE, as expected. Regions of negative $\varepsilon_{\theta_{ei}}$ are found where $z_r < z$, which occurs mostly at upper levels but also in a few surface parcels, which are negatively buoyant with respect to the environmental sounding. For these parcels, an increase in θ_{ei} results in a decrease in APE density.

The efficiency ε_{r_t} is generally negative below $z = 15$km for two reasons. Firstly, the moist air buoyancy (4) contains negative contributions from liquid water and ice. This means that for saturated parcels, an increase in r_t will act to increase the water loading, decrease the buoyancy and decrease the APE density. The second reason stems from the addition of water vapour to unsaturated air near the surface, which will become saturated when lifted to its reference height. As documented by Pauluis (2011), lifting unsaturated air to saturation reduces the efficiency of an atmospheric heat engine, because energy must be used to increase the Gibbs free energy of the water vapour (Pauluis terms this the *Gibbs penalty*). Similarly, this effect acts to decrease APE density.

It is important to note that some physical processes act to influence the APE density through changes in both θ_{ei} and r_t, and their effects should not be assessed without considering the sum of the two production terms (since the partitioning depends on the choice of conserved variables). For example, precipitation of liquid water out of parcels in the lower atmosphere acts to increase APE through the r_t term, by reducing the water loading, but decreases APE through the θ_{ei} term because the latent heat of fusion that could have been released if the parcel were lifted to its freezing level is now lost. The surface flux of water vapour increases APE by adding latent heat through the θ_{ei} term, but decreases APE due to the Gibbs penalty. For this reason, only the total diabatic APE production will be shown in the budget, rather than breaking it down into θ_{ei} and r_t components.

When the APE budget (30) is integrated over the whole model domain, the chief budget contributor is the effect of spatial discontinuities in e_a (not shown). This makes the budget difficult to interpret physically; it was discussed in Section 3 that the physical relevance of spatial discontinuities in e_a is unclear. Discontinuities in e_a are not likely to result in discontinuities in velocity.

Instead of considering the whole domain, the focus of the APE budget is therefore narrowed to the inner radial regions, where the majority of the generation of kinetic energy is expected to occur. In Figure 8, the budget of APE density is integrated over a cylinder of radius 300 km around the

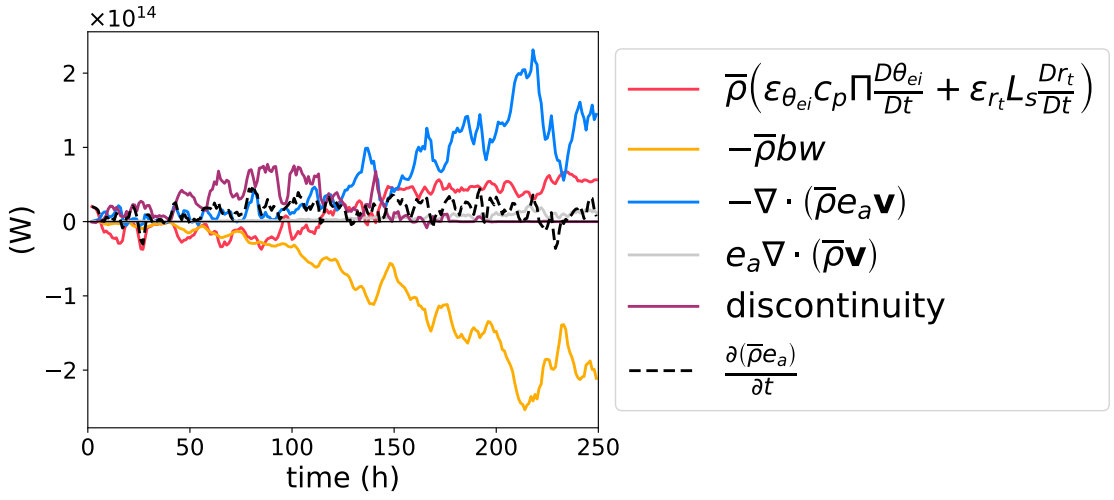

FIG. 8: APE budget (30) integrated over all grid points in the inner region (within $r = 300$ km of the TC centre). Time series have been smoothed using a 3 h running mean. The horizontal black line marks 0 W.

centre of the cyclone. This radial threshold is chosen such that all surface hurricane-force winds ($v > 33\,\mathrm{m\,s^{-1}}$) are included within the region considered. This subset of the domain will henceforth be referred to as the *inner region*.

In the inner region of the TC, spatial discontinuities still dominate during the early stages of development, so it is difficult to use the APE budget to draw any conclusions about the intensification process. This points to a significant limitation of the local APE budget using the initial sounding reference state, which is that its physical meaning only becomes clear once the TC is generally warmer than the initialisation sounding. It can be seen from Figure 8 that after 150 h, once the TC has reached maturity, the contribution of spatial discontinuities to the budget becomes small in the inner region, since all lower-level parcels have become positively buoyant relative to the initial sounding.

After 150 h, the predominant source of APE in the inner region is the flux of APE into the region. This is dependent on the choice of the size of the region: for larger inner regions, the inward flux becomes smaller and diabatic production within the region becomes more important. The vertical profile of the flux of APE across the $r = 300\,\mathrm{km}$ surface at 200 hours (Figure 9) shows that this flux enters through the low-level radial inflow, with very little exported at upper levels.

In the TC's mature stage, the sum of the influx of APE into the region and the local diabatic production is approximately balanced by the conversion of APE to kinetic energy, demonstrating

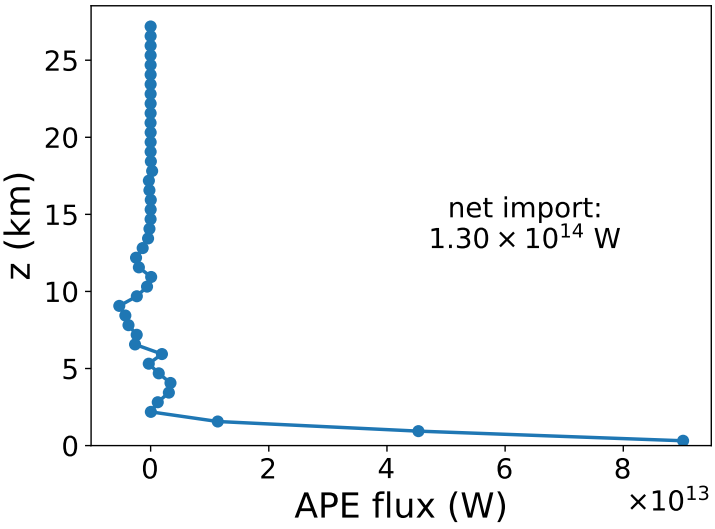

FIG. 9: Flux of APE across the $r = 300$ km surface at 200 h. Blue circles indicate the ν-grid vertical levels, at which the flux is calculated. Positive values correspond to an influx of APE to the inner region at that vertical level, while negative values correspond to an outward flux.

that the definition of the APE as "available" for conversion to kinetic energy is reasonable in this region—the definition reasonably estimates the portion of the potential energy that is actually available to be converted into kinetic energy.

We conclude that in this mature tropical cyclone simulation, the diabatic production of APE in the inner region is less important to the production of kinetic energy than the transport of APE into the region by the secondary circulation. To confirm where and how this transported APE is originally produced, we look at the total diabatic APE production at all grid points in the domain at 200 hours (Figure 10). The majority of APE production occurs in the lowest model level. The APE production is largest in parcels at 1000–1500 km, partly because parcels at larger radii represent a larger volume over which APE can be produced.

To determine the processes that produce the APE that is ultimately transported to the inner region, we integrate the total diabatic production over the inflow region shown by the dashed box in Figure 10 (which has its inner radial boundary at $r = 300$ km), at each time step. This produces the budget in Figure 11, where the dashed black line indicates the total APE production by diabatic processes. The APE production by subgrid processes is split into the contribution from surface fluxes and the contribution from internal mixing (the latter being computed by subtracting the surface flux APE production from the total subgrid APE production). This budget confirms

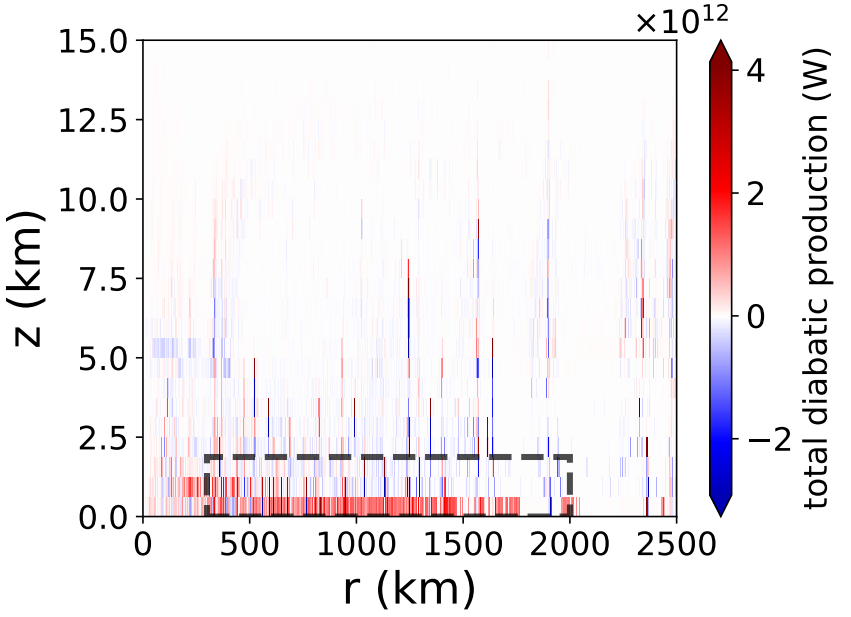

FIG. 10: Total diabatic production of APE at 200 h. Dashed box marks region of inflow integration.

that surface fluxes are the primary source of APE. In the inflow region, mixing acts as a sink of APE, consistent with previous findings of water vapour diffusion as a major sink of APE (Pauluis 2007). Radiative cooling also reduces APE slightly. This demonstrates that the choice of subgrid turbulence parameterisation affects the APE generated in the key production region, and therefore an APE budget could be used to link such parameterisation choices to the energy available for a TC.

The production of APE by surface fluxes in the inflow region is broken down further in Figure 12 to investigate the relative contributions of the sensible and latent heat fluxes. The contribution of the sensible heat flux is small compared to the latent heat flux. The production of APE driven by the surface moisture flux's contribution to latent heat (via the θ_{ei} term) is reduced by about 25% due to the decrease in APE arising from the Gibbs penalty.

Finally, we can link the APE budget for the inner region of the TC to the kinetic + available elastic energy budget, as derived in Equation (10). Figure 13 shows the integral of the kinetic/elastic energy budget over the inner 300 km of the domain. Note that since the $\overline{\rho} bw$ term is the conversion of APE to KE, it appears with identical magnitude but opposite sign in Figures 8 and 13.

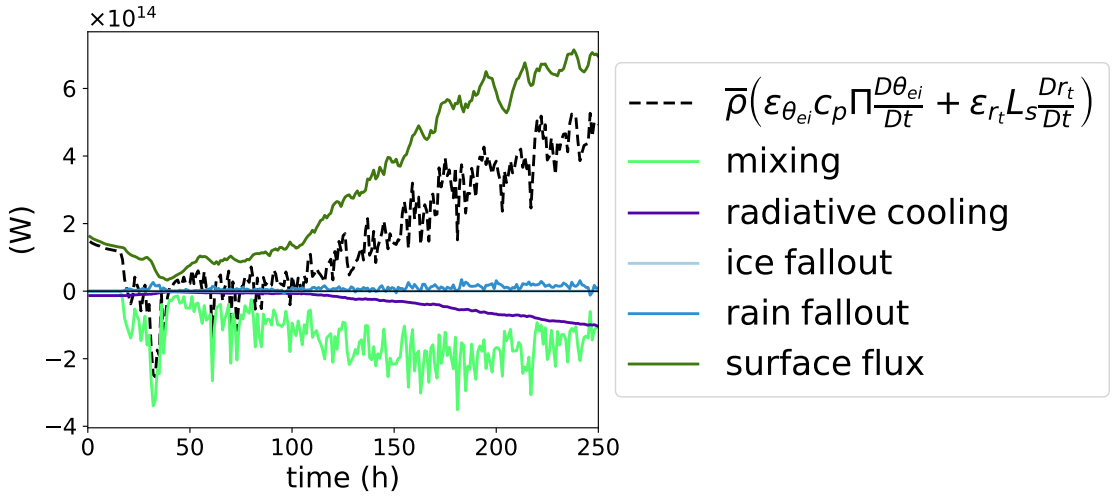

FIG. 11: Components of total diabatic production of APE in inflow region. The horizontal black line marks 0 W.

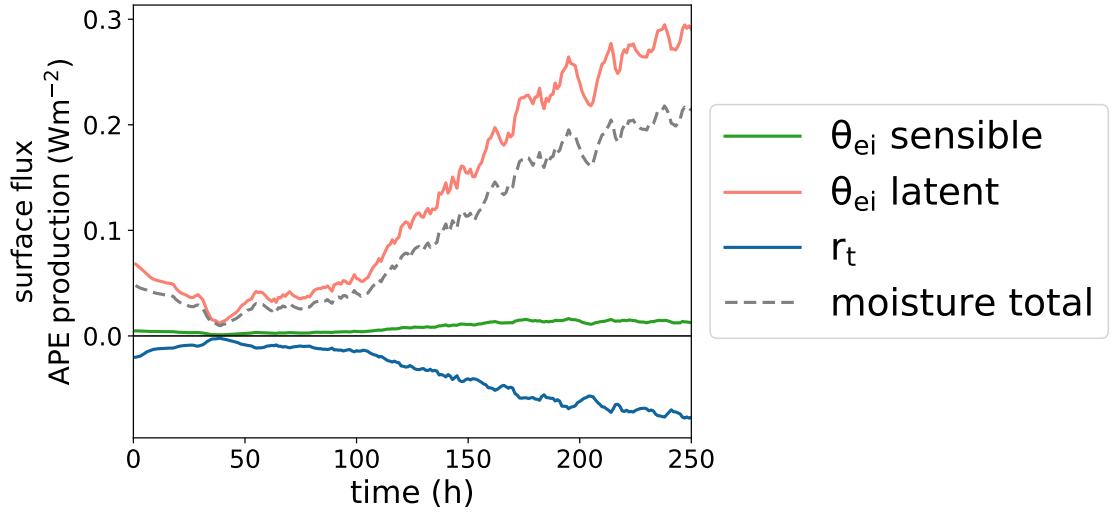

FIG. 12: Contributions to APE production by components of surface flux, integrated over inflow region. The grey dashed line shows the total APE production by surface fluxes of r_v, combining their effects through the θ_{ei} and r_t production terms. The horizontal black line marks 0 W m^{-2}.

Once APE is converted to KE in the inner region, it is mostly exported as mechanical energy. Almost all the export of mechanical energy occurs through the $c_p\overline{\theta_v}\pi$ term, so it is due to pressure work on the volume boundary rather than the transport of kinetic energy out of the region. Some kinetic energy is also dissipated by friction within the inner region.

The overall picture of the energetics in the inner region of the axisymmetric model's mature TC is now complete: APE is produced by surface fluxes of latent heat outside the inner region and

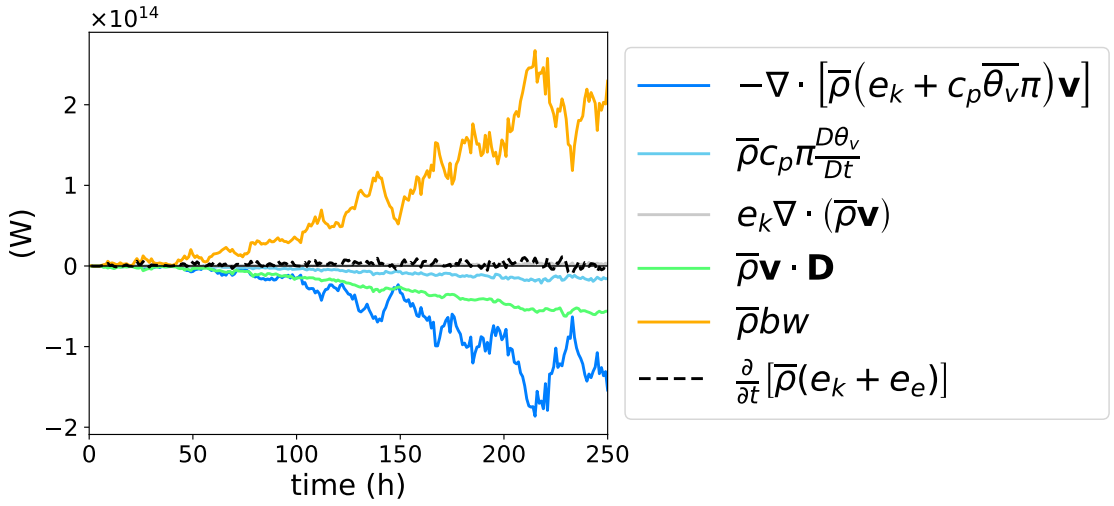

FIG. 13: Kinetic plus available elastic energy budget for inner region. The horizontal black line marks 0 W.

transported into the core by the low-level radial inflow; it is then converted into kinetic energy by vertical buoyancy fluxes, some is dissipated by friction, and the remainder is exported as mechanical energy via pressure work on the region boundary.

a. Moist APE density and Potential Intensity

It is noticeable that the maximum efficiency $\varepsilon_{\theta_{ei}}$ in Figure 7a is similar to the value of $\frac{1}{3}$ traditionally quoted as the approximate value of the Carnot efficiency in potential intensity (PI) theory, as described in Section 1. It is therefore of interest to understand the physical links between moist APE and PI theories. This section derives an equation for PI based on local moist APE theory and compares it to existing theories of PI.

To do this, we discard the approximations made for the axisymmetric model and use the exact compressible theory from Tailleux (2018). Using the moist entropy s and total specific humidity q_t as our conserved variables, the production efficiencies are $G_s = T - T_r$ and $G_{q_t} = \mu - \mu_r$ (here the efficiencies apply to the production of the sum of APE and available elastic energy). Since we know that the chief diabatic process generating APE is surface fluxes, we assume that the maximum wind speed is found by balancing the generation of available energy by surface fluxes with the

frictional dissipation of KE,

$$C_k \left|\vec{v}_S\right| \left[G_s \left(s^* - s\right) + G_{q_t} \left(q_v^* - q_v\right)\right] = C_D \left|\vec{v}_S\right|^3, \tag{31}$$

where $\vec{v}_S = \sqrt{u^2 + v^2}$ is the surface wind speed. All quantities are evaluated in the boundary layer in the region of highest winds, except starred quantities, which are evaluated at saturation at the sea surface. Here we have assumed the usual bulk formulae for surface fluxes and stresses.

Equation (31) can be rearranged to obtain the potential intensity

$$v_{\max}^2 = \frac{C_k}{C_D} \left[G_s \left(s^* - s\right) + G_{q_t} \left(q_v^* - q_v\right)\right]. \tag{32}$$

If we neglect the contribution from APE production by q_t, substitute the form of G_s, and write $s = c_p \ln \theta_e$, we obtain

$$v_{\max}^2 = c_p \left(T - T_r\right) \frac{C_k}{C_D} \left(\ln \theta_e^* - \ln \theta_e\right), \tag{33}$$

which is identical to Equation (1) of Bister and Emanuel (2002), other than the omission of the factor due to dissipative heating and the use of the reference temperature T_r in place of the mean outflow temperature T_0. This is equivalent to calculating the outflow temperature by assuming that outflow occurs at a parcel's level of neutral buoyancy with respect to the reference state; a similar approach was originally suggested by Emanuel (1986), although it was not framed in terms of APE theory. Therefore, APE efficiencies derived from the full moist local framework can be linked to existing TC potential intensity theory in a way that efficiencies based on TPE or dry APE cannot. The relationship between moist APE and potential intensity is also likely connected to the CAPE-based formulation of PI (Bister and Emanuel 2002), which does not neglect the term proportional to $\left(q_v^* - q_v\right)$ (Rousseau-Rizzi et al. 2022).

The maximum APE efficiency G_s performs the same role in APE theory as the Carnot efficiency in traditional PI theory. However, APE theory does not require the assumption of a closed thermodynamic cycle; APE efficiencies are defined for any moist air parcel regardless of its trajectory or whether the TC is in a steady state. It is therefore easier to use APE theory to investigate the temporally- and spatially-varying efficiency of a TC.

5. Discussion and Conclusions

We have demonstrated that it is possible to construct a budget of moist Available Potential Energy for a TC, based on the local formulation of APE theory. This allows a complete budget of the available energetics, down to the diabatic processes responsible for generating APE. In the mature TC simulated by the axisymmetric model, the main source of APE production is latent surface heat flux. The production of APE occurs mostly in the outer part of the TC, and the APE is then advected into the inner region of the storm where it is converted to kinetic energy.

One of the main findings in terms of the practical implementation of local APE theory is that APE density is not necessarily a continuous function of space and time; discontinuities in e_a can contribute significantly to the budget. This provides an obstacle to interpreting TC intensification in terms of APE theory, but it is a major fundamental result for local APE theory itself. Discontinuities are likely to play a larger role if the reference state exhibits conditional instability, as this allows parcels to have one level of neutral buoyancy much higher than another. The energy transfers that occur in the presence of discontinuities can be understood by introducing the concept of latent APE. This is the portion of the BPE that could become APE via a discontinuous transition in reference height, rather than only via continuous evolution through diabatic processes.

Temporal discontinuities in reference pressure p_{ref} were recognised by Pauluis (2007) to occur in the Lorenz APE theory, in which the reference state is obtained by adiabatic rearrangement of the domain. However, in that case, the term arising from changes in p_{ref} was shown to vanish when integrated over the whole atmospheric domain, due to the fact that the Lorenz reference state minimises total static energy. In the case of local APE theory, since APE density is calculated independently for each moist air parcel, there is no such guarantee of cancellation over a domain. Therefore, whilst local APE theory brings the advantages that a cheaper reference state can be used and the local energy conversions can be investigated, its main disadvantage may be the need to consider discontinuities in reference height and therefore in APE density.

From a theoretical viewpoint, it may be possible to produce a completely discontinuity-free budget of APE density if an exact thermodynamic framework were employed and a conditionally neutral sounding were used as a reference state, since multiple LNBs could no longer exist. However, this is unlikely to be practical from a numerical modelling perspective. We constructed APE budgets for runs of the axisymmetric model initialised with the neutral environmental sounding developed by

Rotunno and Emanuel (1987); this is a modified version of the Jordan sounding, which is designed to be neutral to moist convection for an SST of 26.3°C. Small discontinuity terms were achieved with the neutral sounding for SSTs of 26.3°C, 28.3°C and 30.3°C runs, but discontinuities were not eliminated from the budget entirely, even in the mature stage. This suggests that discontinuities in local APE budgets may be inevitable for numerical models of the moist atmosphere, due to their thermodynamic approximations and discretised nature. The budgets using the neutral sounding yielded the same conclusions as seen in Section 3. Implementing budgets for these other runs required adapting the size of the inner region to account for differences in TC size, and altering $\widetilde{\Pi}$ to better represent the effective pressure at which APE production occurs in the runs. Attempts to use SSTs of 26.3°C and 28.3°C with the Jordan sounding resulted in large contributions from spatial discontinuities throughout the run, even when integrating over very small inner regions.

Our finding that the influx of APE to the core region is a larger contributor to the APE budget than local diabatic production makes sense in the context of the results of previous TC budgets. The latent energy budgets performed on numerical simulations by Kurihara (1975); Tuleya and Kurihara (1975) showed that in the inner area of their TC, evaporation was negligible compared to moisture flux convergence. Since the majority of APE is being generated by surface fluxes of moisture, the dominance of APE flux convergence in our results is the equivalent of this. The dominance of moisture convergence over local evaporation can also be seen in budgets of more realistic, three-dimensional TC simulations (Trenberth et al. 2007; Yang et al. 2011; Fritz and Wang 2014).

Previous energy budgets based on both TC observations and numerical simulations noted large exports of total potential energy at upper levels (Palmén and Riehl 1957; Kurihara 1975; Tuleya and Kurihara 1975), and Anthes (1974) suggested that the export of heat at high levels could result in a large APE boundary flux. In contrast, when using the local APE framework we see relatively little export of APE at higher levels compared to the import at lower levels, since parcels in the outflow are much closer to their reference heights and therefore have less APE density. Considering only the available energetics rather than the total energetics leads to the conclusion that the export of energy from inner regions of the TC is due to pressure work at the region boundary rather than simply the transport of TPE away from the centre. The small APE export demonstrates that the vast majority of the imported APE is either converted to kinetic energy or stored in the warm core

vortex; both of these options are related to a strengthening of the TC (in the case of the warm core storage, this is not an instantaneous strengthening of wind speed, but would be associated with a drop in central pressure and an increase in the reservoir of APE that may be converted to kinetic energy at a later time). Therefore the APE supplied to the inner region contributes directly to intensification, whereas much of the latent energy supplied to the inner region does not directly contribute to the increase of kinetic energy, since it is simply converted to TPE and then exported back out of the region at upper levels.

The interpretation of the source of APE in a TC differs between the full moist APE theory and APE theories based on the dry potential temperature θ. We have shown that the latent surface heat flux is the key generator of APE, whereas in a dry framework the source of APE appears to be the latent heat released during condensation, similarly to the TPE-based framework (Anthes and Johnson 1968; Edmon Jr and Vincent 1979; Nolan et al. 2007). One advantage offered by the viewpoint of the moist approach is that the efficiency of APE generation can be used to link available energetics to the widely established theory of potential intensity (PI). Whereas the maximum TPE or dry APE efficiency is typically on the order of 5%, occurring in the mid-troposphere (Edmon Jr and Vincent 1979; Hack and Schubert 1986), the maximum moist APE efficiency occurs in near-surface parcels and is similar to the Carnot efficiency typically used in PI theory. Local moist APE efficiencies therefore provide a unified way to view temporally- and spatially-varying efficiencies throughout the TC and also the efficiency leading to maximum intensity.

Increases in energetic efficiencies during intensification have been suggested to contribute to the rapid development of TCs (Schubert and Hack 1982; Hack and Schubert 1986; Vigh and Schubert 2009), but these efficiencies were based on the conversion of TPE to KE. Future work will investigate the development of the APE efficiency of boundary layer parcels during intensification, as this can directly explore the effect of boundary layer thermodynamics on a parcel's efficiency, which was not possible using previous energetic efficiency paradigms (Smith and Montgomery 2016).

However, since the definition of local moist APE efficiency is dependent on the choice of reference state, more work needs to be done to explore the suitability of particular reference states. This work has not addressed the possibility of choosing different reference states; since the axisymmetric model momentum equations are defined using the initial environmental sounding, using this as the reference state meant that our definition of APE to vertical KE conversion matched the effective

source of kinetic plus elastic energy in the model. However, the partitioning between the buoyancy term and the vertical pressure gradient term in the vertical momentum equation is non-unique, since it depends on an arbitrary reference state, which is only fixed in the case of a particular model based on reference-state equations. It would therefore be preferable to measure APE to KE conversion independently of reference state. Future work will use the methods developed in this paper for constructing a closed moist APE budget to address the question of whether there is an optimal choice of reference state for defining APE in a TC.

The link between PI and APE is clear when using the exact local available energetics of Tailleux (2018): the traditional PI equation of Bister and Emanuel (2002) is the same as Equation (33) derived from moist local APE theory, using the reference temperature T_r (which is calculated as the LNB—relative to the reference state—of a surface parcel) instead of the outflow temperature T_{out} in the efficiency. Using an LNB with respect to the initial environmental sounding has been suggested in the past as a method of calculating T_{out} (Emanuel 1986; Rotunno and Emanuel 1987), although the link to APE was not made.

Potential intensity theory is often understood in terms of entropy, by treating the TC as a heat engine (Emanuel 1988). The interpretation of the effect of irreversible processes on TC intensification may differ between an APE budget and an entropy budget. Whereas irreversible processes must be a source of entropy by definition, they can be either a source or a sink of APE depending on the signs of the APE production efficiencies. That irreversible processes can promote intensification is already well-established in the case of dissipative heating; since most of this heating occurs in the boundary layer in the region of maximum wind, it is recycled as an energy source to the TC (Bister and Emanuel 1998). From the APE viewpoint, dissipative heating is a source of APE because it is a source of entropy in parcels with positive $G_s = T - T_r$.

Other irreversible processes are often just considered as entropy sources that decrease the Carnot efficiency of a TC, reducing its PI. For example, Sabuwala et al. (2015) treated the frictional dissipation in the wake of falling raindrops ("rainpower") in this manner. However, whether rainpower provides a source or sink of APE would depend on the sign of G_s in the parcel in which the frictional dissipation occurred. The effect of an irreversible process on intensification or maximum intensity should include a consideration of the efficiency at which it occurs. Establishing the impact of the choice of reference state is particularly important for the study of irreversible

processes; a given process could be a source of APE with respect to one reference state and a sink of APE with respect to another.

Since the local APE budget links processes involving moisture and convection to the ultimate intensification of TCs, it has the potential to provide a useful diagnostic tool with which to investigate the processes affecting the intensity distributions of TCs produced by climate models. However, there are still difficulties to be overcome in order to achieve this. Most notably, we were only able to draw useful physical conclusions about the APE budget in the mature stage of the simulated axisymmetric TC, with the effects of discontinuities posing an obstacle during the intensification stage. It would therefore be desirable to develop APE diagnostics that are less affected by the presence of discontinuities in APE density, in order to investigate the budget during the development stage of TCs.

We have also only investigated the budget for an idealised axisymmetric model with an easily defined reference state. To develop the budget for non-axisymmetric models, a sensible intermediate step would be to analyse azimuthally-averaged data in order to facilitate comparison with the results here, with possible study of asymmetric effects following later. Reference states could be calculated in more complex models using a time-varying profile at some distance from the cyclone centre (scaled according to the TC size), to represent the ambient conditions.

Where it is too difficult or computationally expensive to construct a full closed APE budget, or where discontinuities prevent a satisfactory physical interpretation, some partial aspects of the budget are easier to investigate and could provide valuable physical insight. For example, calculating the APE production efficiency of surface parcels requires only a reference sounding and surface fields of temperature, pressure and water vapour mixing ratio. As a further simplification, the exact analytic forms of the efficiencies could be used rather than strictly using the model's conserved variables and thermodynamic approximations. For the axisymmetric TC analysed in this paper, the flux of moist APE into the TC core at low levels is linked to the total conversion of APE to kinetic energy in the core. Therefore, evaluating this flux could provide a diagnostic linked to the integrated kinetic energy produced by a TC.

Differences between the integrated conversion of APE to kinetic energy via vertical buoyancy fluxes in the core (again using the environmental reference state) could also be of interest; this is likely to be useful for investigating differences caused by convection schemes, since the buoyancy

fluxes occur as a result of convection. For example, two models with different convection schemes could produce the same APE through surface fluxes, and import the same amount of APE into the core, but then convert a different amount of this imported APE into kinetic energy, resulting in different intensities.

A full budget of APE production rate, similar to the one shown in Figure 11, could provide insights into the energetic effects of diabatic processes in TCs, although due to the effects of discontinuities it is unlikely to be physically interpretable during the intensification stage. It would be particularly helpful if the APE production rate could be verified to match the model's rate of kinetic energy generation. Such a budget is more ambitious, since it requires all diabatic processes in the model to be accounted for, and to have full spatial fields of their tendency terms available. The budget could assess, for example, how a change in the microphysics scheme affects the generation of APE by precipitation, or how changes in mixing length alter the contribution from subgrid turbulence.

Acknowledgments. B.L.H. was funded by NERC as part of the SCENARIO Doctoral Training Partnership (NE/L002566/1). We would like to thank Brian Tang and an anonymous reviewer for their valuable suggestions for improving the manuscript.

Data availability statement. The code used to run the axisymmetric model and compute the budgets described in this paper are available at `https://github.com/bethanharris/tropical-cyclone-energetics`.

APPENDIX A

Discretisation of APE budget

The expressions for APE density e_a and efficiencies $G_{\theta_{ei}}, G_{r_t}$ were given in Section 3 by Equations (22), (24), (25). However, to obtain a closed local APE budget for the axisymmetric model, it is necessary to modify these forms to account for the model's thermodynamic approximations, and to discretise them onto the model grid. Here, we briefly describe the grid that the model uses, and give the forms for the discretised APE density and efficiencies.

The axisymmetric model is structured on an Arakawa C-grid, with the velocity components u, v and w all computed at different points. The grid is shown in Figure A1. All thermodynamic variables (e.g. $\theta, r_j, \Pi, \overline{\rho}$) are computed at v-points. When computing buoyancy for use in the vertical momentum equation, b is required at w-points, which is achieved by linear interpolation of $\theta, r_j, \overline{\theta}, \overline{r_j}$ to the w-levels.

Since all other thermodynamic variables are defined at v-points, it is desirable for our APE density to be defined at v-points. We also impose the requirement that our discretised APE density satisfies an analog of

$$\left(\frac{\partial e_a}{\partial z}\right)_{\theta_{ei}, r_t} = -b, \tag{A1}$$

since it is this property that yields the form $-bw$ for the conversion of APE to kinetic energy, which is crucial for our understanding of the link between the APE budget and TC intensification. We ignore for the moment the possibility of discontinuities in z_r.

Using the initial model vertical profile as our reference state, we interpolate $\overline{\theta}, \overline{r_v}, \overline{\Pi}$ so that we have a reference profile for each defined at all v- and w- levels. Each parcel's buoyancy (4) is computed at every level of the reference profile $\overline{\Pi}(z)$, assuming that θ_{ei} and r_t are conserved. Any

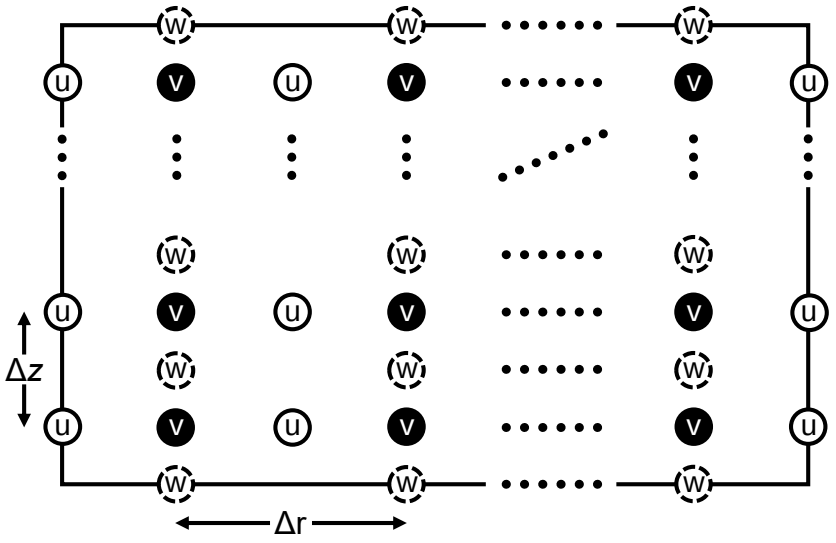

FIG. A1: Axisymmetric model grid structure. The solid black rectangle marks the boundaries of the domain. The components u, v and w of the velocity are computed at the labelled grid points. All thermodynamic variables (e.g. θ, r_v, Π) are computed at the same locations as v. Dots show where the grid pattern repeats.

levels of neutral buoyancy are identified by linear interpolation of the buoyancy between profile points. The nearest LNB in the direction of in situ buoyancy is identified as the reference height z_r.

For a parcel at v-point (i, j, t), we assume that $z_r > z$ (an analogous construction applies for $z_r < z$). If z_r lies between the vertical v-levels n and $n+1$, then we define the parcel's APE density as

$$e_{a_{i,j,t}} = \sum_{k=j}^{n} b_{i,k+\frac{1}{2},t} \Delta z + b_{i,n+\frac{1}{2},t} \left(z_r - z_n\right), \tag{A2}$$

where Δz is the model's vertical grid-spacing. This definition of the APE density obeys

$$\frac{e_{a_{i,j+1,t}} - e_{a_{i,j,t}}}{\Delta z} = -b_{i,j+\frac{1}{2},t}, \tag{A3}$$

which satisfies our requirement for a discretised version of (A1). This also yields b on w-levels as used in the discretised vertical momentum equation. An illustration of the computation of discretised APE density is shown in Figure A2.

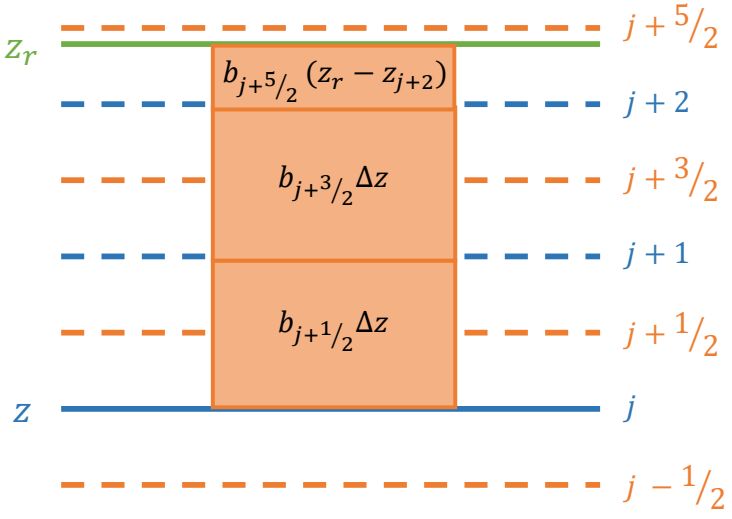

FIG. A2: Schematic of method for computing APE density for a parcel at vertical v-level j with $z_r > z$. Blue lines indicate vertical v-grid levels, which are spaced Δz apart. The solid blue line labelled z shows the parcel's initial position. Orange dashed lines mark vertical levels on the w-grid, which occur midway between v-levels. The green line labelled z_r is the parcel's reference height (chosen arbitrarily for the purposes of the demonstration). The shaded orange boxes show each term contributing to the sum (A2), and are labelled with the term's value (box widths are not proportional to value).

Unlike the continuous version of APE density defined in Eq. (22), which is positive definite, it is possible for the discretised APE density to be negative if $|z_r - z| < \frac{\Delta z}{2}$. However, in such a case the APE density is likely to be small anyway and therefore this possibility is not found to be important for the APE budget over a region.

To obtain the discretised APE production coefficients $G_{\theta_{ei}}$ and G_{r_t} that will give us a closed budget, we start with the forms

$$G_{\theta_{ei}} = \int_z^{z_r} \frac{\partial b}{\partial \theta_{ei}}\,(\theta_{ei}, r_t, z')\,dz', \tag{A4}$$

$$G_{r_t} = \int_z^{z_r} \frac{\partial b}{\partial r_t}\,(\theta_{ei}, r_t, z')\,dz', \tag{A5}$$

(as derived in Equation (23)) and discretise them using the same method as (A2). This leads to

$$G_{\theta_{ei}i,j,t} = \sum_{k=j}^{n} \left.\frac{\partial b}{\partial \theta_{ei}}\right|_{i,k+\frac{1}{2},t} \Delta z + \left.\frac{\partial b}{\partial \theta_{ei}}\right|_{i,n+\frac{1}{2},t} (z_r - z_n)\,, \tag{A6}$$

$$G_{r_t i,j,t} = \sum_{k=j}^{n} \left.\frac{\partial b}{\partial r_t}\right|_{i,k+\frac{1}{2},t} \Delta z + \left.\frac{\partial b}{\partial r_t}\right|_{i,n+\frac{1}{2},t} (z_r - z_n), \tag{A7}$$

for the case $z_r > z$. All that remains to be done to obtain the efficiencies is to find expressions for $\frac{\partial b}{\partial \theta_{ei}}$ and $\frac{\partial b}{\partial r_t}$, using

$$db = \frac{\partial b}{\partial \theta} d\theta + \frac{\partial b}{\partial r_v} dr_v + \frac{\partial b}{\partial r_l} dr_l + \frac{\partial b}{\partial r_i} dr_i + \frac{\partial b}{\partial z} dz, \tag{A8}$$

$$d\theta_{ei} = d\theta + \frac{L_s}{c_p \Pi} dr_v + \frac{L_f}{c_p \Pi} dr_l, \tag{A9}$$

$$dr_t = dr_v + dr_l + dr_i, \tag{A10}$$

where we have included liquid precipitation in r_l. The problem may be split into three cases: where the parcel is unsaturated ($r_l = r_i = 0$, $dr_t = dr_v$), where the parcel is saturated but no freezing has occurred ($r_i = 0, dr_t = dr_l + dr_{vs}$), and where the parcel has undergone freezing ($dr_t = dr_i + dr_{vs}$). We assume for simplicity that if $T < 0°\mathrm{C}$, all liquid freezes to ice. This will overestimate the occurrence of freezing, since in reality some liquid water would continue to exist down to about $-40°\mathrm{C}$.

Eqs. (A8), (A9), (A10) can be rearranged for each of these cases, making use of the Clausius-Clapeyron relation. Defining the factors

$$F_s = \frac{1 + \frac{L_v r_{vs}}{R_d T}}{1 + \frac{\epsilon L_v^2 r_{vs}}{c_p R_d T \theta \Pi}}, \tag{A11}$$

$$F_f = \frac{1 + \frac{L_s r_{vs}}{R_d T}}{1 + \frac{\epsilon L_s^2 r_{vs}}{c_p R_d T \theta \Pi}}, \tag{A12}$$

where $\epsilon = \frac{R_d}{R_v}$, the required partial derivatives are

$$\frac{\partial b}{\partial \theta_{ei}} = \begin{cases} \frac{g}{\theta} & \text{if unsaturated} \\ \frac{g}{\theta} F_s & \text{if saturated}, T > 0°\mathrm{C} \\ \frac{g}{\theta} F_f & \text{if saturated}, T < 0°\mathrm{C}, \end{cases} \tag{A13}$$

$$\frac{\partial b}{\partial r_t} = \begin{cases} g\left(0.61 - \frac{L_s}{c_p \Pi \overline{\theta}}\right) & \text{if unsaturated} \\ -g\left(1 + \frac{L_f}{c_p \Pi \overline{\theta}} F_s\right) & \text{if saturated}, T > 0°\text{C} \\ -g & \text{if saturated}, T < 0°\text{C}. \end{cases} \tag{A14}$$

The use of these expressions in Eqs. (A6), (A7) allows the computation of our discretised APE efficiencies. Although the forms found in this appendix look very different to the exact theoretical forms of the efficiencies found in (24), (25), when used in practice the results are similar.

APPENDIX B

Closure of APE budget

Figure B1 shows the accuracy of the APE budget integrated over the inner region ($r < 300$ km), which was used to generate Figure 8.

The closure of the budget after 150 h, when there are no discontinuities in e_a, is of particular interest. The budget uses a conditional residual to diagnose the contribution by discontinuities, which could lead to an artificially good closure. However, the budget captures the variation in

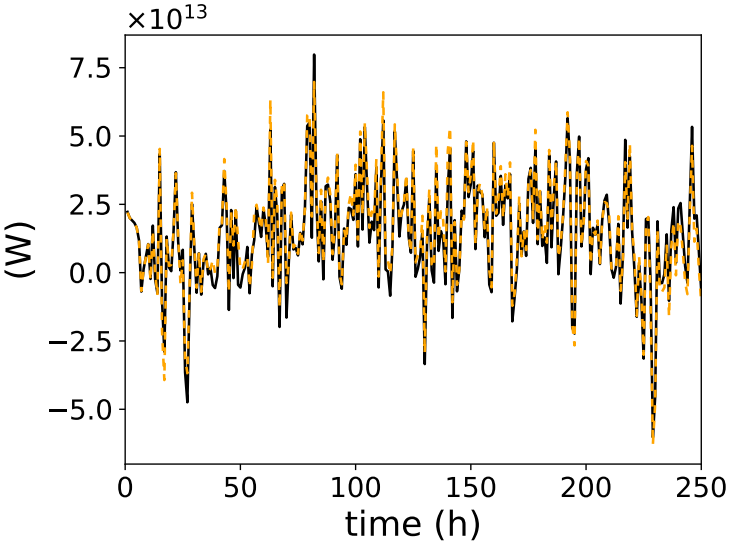

FIG. B1: Accuracy of the APE budget integrated over the inner 300 km of the domain. The solid black line shows the diagnosed $\frac{\partial(\overline{\rho} e_a)}{\partial t}$ from the model, and the dashed orange line shows the sum of the APE budget components.

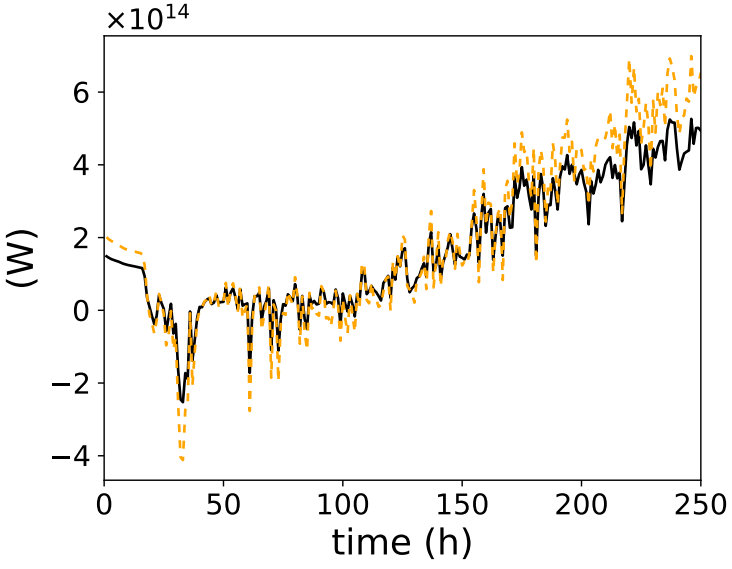

FIG. B2: Accuracy of diabatic APE production budget integrated over inflow region. The solid black line is the production computed using the model-diagnosed Lagrangian derivatives of θ_{ei} and r_t. The orange dashed line is the diabatic production computed as part of the APE budget.

$\frac{\partial(\overline{\rho}e_a)}{\partial t}$ well after 150 h, so we can conclude that the budget is accurate even in the absence of discontinuities and the associated residual calculation.

The budget of diabatic APE production in the inflow region can also be verified; this was presented in Figure 11. The black solid line in Figure B2 is the value of $\overline{\rho}\varepsilon_{\theta_{ei}} c_p \Pi \frac{D\theta_{ei}}{Dt} + \overline{\rho}\varepsilon_{r_t} L_s \frac{Dr_t}{Dt}$ diagnosed using material derivatives diagnosed from the model (i.e. not breaking the production down into individual diabatic processes, and not using the averaged pressure $\widetilde{\Pi}$ as described in Section 3). The orange dashed line is the sum of diabatic APE production computed for all the diabatic processes in the APE budget. This employs the domain-averaged $\widetilde{\Pi}$ to compute θ_{ei} and hence $\frac{D\theta_{ei}}{Dt}$, in order to account for the neglect of variations in Π in the model's Lagrangian derivative of θ_{ei}. Figure B2 demonstrates that the production calculated by the two methods is similar; the APE budget provides an overestimate of production towards the end of the model run, but the overall trend is consistent with the APE production by surface fluxes increasing until it dominates over the loss due to mixing. The discrepancies are due to the use of $\widetilde{\Pi}$ rather than errors in budgeting $\frac{D\theta_{ei}}{Dt}$ or $\frac{Dr_t}{Dt}$.

References

Andrews, D. G., 1981: A note on potential energy density in a stratified compressible fluid. *J. Fluid Mech.*, **107**, 227–236, https://doi.org/10.1017/S0022112081001754.

Anthes, R. A., 1974: The dynamics and energetics of mature tropical cyclones. *Rev. Geophys.*, **12 (3)**, 495–522, https://doi.org/10.1029/RG012i003p00495.

Anthes, R. A., and D. R. Johnson, 1968: Generation of Available Potential Energy in Hurricane Hilda (1964). *Mon. Wea. Rev.*, **96 (5)**, 291–302, https://doi.org/10.1175/1520-0493(1968)096<0291:GOAPEI>2.0.CO;2.

Bannon, P. R., 2003: Hamiltonian Description of Idealized Binary Geophysical Fluids. *J. Atmos. Sci.*, **60 (22)**, 2809–2819, https://doi.org/10.1175/1520-0469(2003)060<2809:HDOIBG>2.0.CO;2.

Bister, M., and K. A. Emanuel, 1998: Dissipative heating and hurricane intensity. *Meteor. Atmos. Phys.*, **65 (3-4)**, 233–240, https://doi.org/10.1007/BF01030791.

Bister, M., and K. A. Emanuel, 2002: Low frequency variability of tropical cyclone potential intensity 1. Interannual to interdecadal variability. *J. Geophys. Res.*, **107 (D24)**, 4801, https://doi.org/10.1029/2001JD000776.

Bryan, G. H., and R. Rotunno, 2009: The Maximum Intensity of Tropical Cyclones in Axisymmetric Numerical Model Simulations. *Mon. Wea. Rev.*, **137 (6)**, 1770–1789, https://doi.org/10.1175/2008MWR2709.1.

Craig, G. C., 1995: Radiation and polar lows. *Quart. J. Roy. Meteor. Soc.*, **121 (521)**, 79–94, https://doi.org/10.1002/qj.49712152105.

Craig, G. C., 1996: Numerical experiments on radiation and tropical cyclones. *Quart. J. Roy. Meteor. Soc.*, **122 (530)**, 415–422, https://doi.org/10.1002/qj.49712253006.

Edmon Jr, H. J., and D. G. Vincent, 1979: Large-Scale Atmospheric Conditions During the Intensification of Hurricane Carmen (1974) II. Diabatic Heating Rates and Energy Budgets. *Mon. Wea. Rev.*, **107 (3)**, 295–313, https://doi.org/10.1175/1520-0493(1979)107<0295:LSACDT>2.0.CO;2.

Emanuel, K., 1986: An Air-Sea Interaction Theory for Tropical Cyclones. Part I: Steady-State Maintenance. *J. Atmos. Sci.*, **43 (6)**, 585–605, https://doi.org/10.1175/1520-0469(1986)043<0585:AASITF>2.0.CO;2.

Emanuel, K., 2003: Tropical Cyclones. *Annu. Rev. Earth Planet. Sci.*, **31 (1)**, 75–104, https://doi.org/10.1146/annurev.earth.31.100901.141259.

Emanuel, K. A., 1987: The dependence of hurricane intensity on climate. *Nature*, **326 (6112)**, 483–485, https://doi.org/10.1038/326483a0.

Emanuel, K. A., 1988: The Maximum Intensity of Hurricanes. *J. Atmos. Sci.*, **45 (7)**, 1143–1155, https://doi.org/10.1175/1520-0469(1988)045<1143:TMIOH>2.0.CO;2.

Emanuel, K. A., 1994: *Atmospheric Convection*. Oxford University Press, Oxford.

Emanuel, K. A., 1997: Some Aspects of Hurricane Inner-Core Dynamics and Energetics. *J. Atmos. Sci.*, **54 (8)**, 1014–1026, https://doi.org/10.1175/1520-0469(1997)054<1014:SAOHIC>2.0.CO;2.

Emanuel, K. A., and R. Rotunno, 1989: Polar lows as arctic hurricanes. *Tellus*, **41A (1)**, 1–17, https://doi.org/10.3402/tellusa.v41i1.11817.

Fritz, C., and Z. Wang, 2014: Water Vapor Budget in a Developing Tropical Cyclone and Its Implication for Tropical Cyclone Formation. *J. Atmos. Sci.*, **71 (11)**, 4321–4332, https://doi.org/10.1175/JAS-D-13-0378.1.

Gill, A. E., 1982: *Atmosphere-ocean dynamics*. Academic Press, 662 pp.

Hack, J. J., and W. H. Schubert, 1986: Nonlinear Response of Atmospheric Vortices to Heating by Organized Cumulus Convection. *J. Atmos. Sci.*, **43 (15)**, 1559–1573, https://doi.org/10.1175/1520-0469(1986)043<1559:NROAVT>2.0.CO;2.

Harris, B. L., and R. Tailleux, 2018: Assessment of algorithms for computing moist available potential energy. *Quart. J. Roy. Meteor. Soc.*, **144**, 1501–1510, https://doi.org/10.1002/qj.3297.

Hogsett, W., and D.-L. Zhang, 2009: Numerical Simulation of Hurricane Bonnie (1998). Part III: Energetics. *J. Atmos. Sci.*, **66 (9)**, 2678–2696, https://doi.org/10.1175/2009JAS3087.1.

Holliday, D., and M. E. McIntyre, 1981: On potential energy density in an incompressible, stratified fluid. *J. Fluid Mech.*, **107**, 221–225, https://doi.org/10.1017/S0022112081001742.

Jordan, C. L., 1958: Mean Soundings for the West Indies Area. *Journal of Meteorology*, **15 (1)**, 91–97, https://doi.org/10.1175/1520-0469(1958)015<0091:MSFTWI>2.0.CO;2.

Kaplan, J., M. DeMaria, and J. A. Knaff, 2010: A Revised Tropical Cyclone Rapid Intensification Index for the Atlantic and Eastern North Pacific Basins. *Wea. Forecasting*, **25 (1)**, 220–241, https://doi.org/10.1175/2009WAF2222280.1.

Kilroy, G., R. K. Smith, and M. T. Montgomery, 2016: Why Do Model Tropical Cyclones Grow Progressively in Size and Decay in Intensity after Reaching Maturity? *J. Atmos. Sci.*, **73 (2)**, 487–503, https://doi.org/10.1175/JAS-D-15-0157.1.

Kim, D., A. H. Sobel, A. D. Del Genio, Y. Chen, S. J. Camargo, M.-S. Yao, M. Kelley, and L. Nazarenko, 2012: The Tropical Subseasonal Variability Simulated in the NASA GISS General Circulation Model. *J. Climate*, **25 (13)**, 4641–4659, https://doi.org/10.1175/JCLI-D-11-00447.1.

Kim, D., and Coauthors, 2018: Process-Oriented Diagnosis of Tropical Cyclones in High-Resolution GCMs. *J. Climate*, **31 (5)**, 1685–1702, https://doi.org/10.1175/JCLI-D-17-0269.1.

Kleinschmidt, E., 1951: Grundlagen einer Theorie der tropischen Zyklonen. *Archiv für Meteorologie, Geophysik und Bioklimatologie Serie A*, **4 (1)**, 53–72, https://doi.org/10.1007/BF02246793.

Klemp, J. B., and R. B. Wilhelmson, 1978: The Simulation of Three-Dimensional Convective Storm Dynamics. *J. Atmos. Sci.*, **35 (6)**, 1070–1096, https://doi.org/10.1175/1520-0469(1978)035<1070:TSOTDC>2.0.CO;2.

Kurihara, Y., 1975: Budget Analysis of a Tropical Cyclone Simulated in an Axisymmetric Numerical Model. *J. Atmos. Sci.*, **32 (1)**, 25–59, https://doi.org/10.1175/1520-0469(1975)032<0025:BAOATC>2.0.CO;2.

Lee, C.-Y., M. K. Tippett, A. H. Sobel, and S. J. Camargo, 2016: Rapid intensification and the bimodal distribution of tropical cyclone intensity. *Nature Communications*, **7**, 10 625, https://doi.org/10.1038/ncomms10625.

970 Lim, Y.-K., S. D. Schubert, O. Reale, M.-I. Lee, A. M. Molod, and M. J. Suarez, 2015: Sensitivity
971 of Tropical Cyclones to Parameterized Convection in the NASA GEOS-5 Model. *J. Climate*,
972 **28 (2)**, 551–573, https://doi.org/10.1175/JCLI-D-14-00104.1.

973 Lorenz, E. N., 1955: Available potential energy and the maintenance of the general circulation.
974 *Tellus*, **7 (2)**, 157–167, https://doi.org/10.3402/tellusa.v7i2.8796.

975 Lorenz, E. N., 1978: Available energy and the maintenance of a moist circulation. *Tellus*, **30 (1)**,
976 15–31, https://doi.org/10.3402/tellusa.v30i1.10308.

977 Lorenz, E. N., 1979: Numerical evaluation of moist available energy. *Tellus*, **31 (3)**, 230–235,
978 https://doi.org/10.3402/tellusa.v31i3.10429.

979 Manganello, J. V., and Coauthors, 2012: Tropical Cyclone Climatology in a 10-km Global Atmo-
980 spheric GCM: Toward Weather-Resolving Climate Modeling. *J. Climate*, **25 (11)**, 3867–3893,
981 https://doi.org/10.1175/JCLI-D-11-00346.1.

982 Marks, F. D., L. K. Shay, and PDT-5, 1998: Landfalling Tropical Cyclones: Forecast Problems and
983 Associated Research Opportunities. *Bull. Amer. Meteor. Soc.*, **79 (2)**, 305–323, https://doi.org/
984 10.1175/1520-0477(1998)079<0285:QPFROT>2.0.CO;2.

985 Moon, Y., and Coauthors, 2019: Azimuthally Averaged Wind and Thermodynamic Structures of
986 Tropical Cyclones in Global Climate Models and Their Sensitivity to Horizontal Resolution. *J.*
987 *Climate*, **33 (4)**, 1575–1595, https://doi.org/10.1175/JCLI-D-19-0172.1.

988 Murakami, H., R. Mizuta, and E. Shindo, 2012a: Future changes in tropical cyclone activity
989 projected by multi-physics and multi-SST ensemble experiments using the 60-km-mesh MRI-
990 AGCM. *Climate Dyn.*, **39 (9-10)**, 2569–2584, https://doi.org/10.1007/s00382-011-1223-x.

991 Murakami, H., and Coauthors, 2012b: Future Changes in Tropical Cyclone Activity Projected by
992 the New High-Resolution MRI-AGCM. *J. Climate*, **25 (9)**, 3237–3260, https://doi.org/10.1175/
993 JCLI-D-11-00415.1.

994 Nolan, D. S., Y. Moon, and D. P. Stern, 2007: Tropical Cyclone Intensification from Asymmetric
995 Convection: Energetics and Efficiency. *J. Atmos. Sci.*, **64 (10)**, 3377–3405, https://doi.org/
996 10.1175/JAS3988.1.

997 Palmén, E., and C. L. Jordan, 1955: Note on the Release of Kinetic Energy in Tropical Cyclones.
998 *Tellus*, **7 (2)**, 186–188, https://doi.org/10.3402/tellusa.v7i2.8793.

999 Palmén, E., and H. Riehl, 1957: Budget of Angular Momentum and Energy in Tropical Cyclones.
1000 *J. Meteor.*, **14 (2)**, 150–159, https://doi.org/10.1175/1520-0469(1957)014<0150:BOAMAE>2.
1001 0.CO;2.

1002 Pauluis, O., 2007: Sources and Sinks of Available Potential Energy in a Moist Atmosphere. *J.*
1003 *Atmos. Sci.*, **64 (7)**, 2627–2641, https://doi.org/10.1175/JAS3937.1.

1004 Pauluis, O., 2011: Water Vapor and Mechanical Work: A Comparison of Carnot and Steam Cycles.
1005 *J. Atmos. Sci.*, **68 (1)**, 91–102, https://doi.org/10.1175/2010JAS3530.1.

1006 Pauluis, O. M., 2016: The Mean Air Flow as Lagrangian Dynamics Approximation and Its
1007 Application to Moist Convection. *J. Atmos. Sci.*, **73 (11)**, 4407–4425, https://doi.org/10.1175/
1008 JAS-D-15-0284.1.

1009 Peng, J., L. Zhang, and Y. Zhang, 2015: On the Local Available Energetics in a Moist Compressible
1010 Atmosphere. *J. Atmos. Sci.*, **72 (4)**, 1551–1561, https://doi.org/10.1175/JAS-D-14-0181.1.

1011 Persing, J., M. T. Montgomery, J. C. McWilliams, and R. K. Smith, 2013: Asymmetric and
1012 axisymmetric dynamics of tropical cyclones. *Atmos. Chem. Phys.*, **13 (24)**, 12 299–12 341,
1013 https://doi.org/10.5194/acp-13-12299-2013.

1014 Randall, D. A., and J. Wang, 1992: The Moist Available Energy of a Conditionally Unstable At-
1015 mosphere. *J. Atmos. Sci.*, **49 (3)**, 240–255, https://doi.org/10.1175/1520-0469(1992)049<0240:
1016 TMAEOA>2.0.CO;2.

1017 Reed, K. A., J. T. Bacmeister, N. A. Rosenbloom, M. F. Wehner, S. C. Bates, P. H. Lauritzen,
1018 J. E. Truesdale, and C. Hannay, 2015: Impact of the dynamical core on the direct simulation
1019 of tropical cyclones in a high-resolution global model. *Geophys. Res. Lett.*, **42 (9)**, 3603–3608,
1020 https://doi.org/10.1002/2015GL063974.

1021 Reed, K. A., and C. Jablonowski, 2011: Impact of physical parameterizations on idealized trop-
1022 ical cyclones in the Community Atmosphere Model. *Geophys. Res. Lett.*, **38 (4)**, L04 805,
1023 https://doi.org/10.1029/2010GL046297.

Roberts, M. J., and Coauthors, 2015: Tropical Cyclones in the UPSCALE Ensemble of High-Resolution Global Climate Models. *J. Climate*, **28 (2)**, 574–596, https://doi.org/10.1175/JCLI-D-14-00131.1.

Roberts, M. J., and Coauthors, 2020: Impact of model resolution on tropical cyclone simulation using the HighResMIP-PRIMAVERA multi-model ensemble. *J. Climate*, **33 (7)**, 2557–2583, https://doi.org/10.1175/JCLI-D-19-0639.1.

Rotunno, R., and K. Emanuel, 1987: An Air-Sea Interaction Theory for Tropical Cyclones. Part II: Evolutionary Study Using a Nonhydrostatic Axisymmetric Numerical Model. *J. Atmos. Sci.*, **44 (3)**, 542–561, https://doi.org/10.1175/1520-0469(1987)044<0542:AAITFT>2.0.CO;2.

Rousseau-Rizzi, R., and K. Emanuel, 2019: An Evaluation of Hurricane Superintensity in Axisymmetric Numerical Models. *J. Atmos. Sci.*, **76 (6)**, 1697–1708, https://doi.org/10.1175/JAS-D-18-0238.1.

Rousseau-Rizzi, R., T. M. Merlis, and N. Jeevanjee, 2022: The connection between Carnot and CAPE formulations of TC potential intensity. *J. Climate*, **35 (3)**, 941–954, https://doi.org/10.1175/JCLI-D-21-0360.1.

Sabuwala, T., G. Gioia, and P. Chakraborty, 2015: Effect of rainpower on hurricane intensity. *Geophys. Res. Lett.*, **42 (8)**, 3024–3029, https://doi.org/10.1002/2015GL063785.

Saenz, J. A., R. Tailleux, E. D. Butler, G. O. Hughes, and K. I. C. Oliver, 2015: Estimating Lorenz's Reference State in an Ocean with a Nonlinear Equation of State for Seawater. *J. Phys. Oceanogr.*, **45 (5)**, 1242–1257, https://doi.org/10.1175/JPO-D-14-0105.1.

Schmidt, C. W., and R. K. Smith, 2016: Tropical cyclone evolution in a minimal axisymmetric model revisited. *Quart. J. Roy. Meteor. Soc.*, **142 (696)**, 1505–1516, https://doi.org/10.1002/qj.2753.

Schubert, W. H., and J. J. Hack, 1982: Inertial Stability and Tropical Cyclone Development. *J. Atmos. Sci.*, **39 (8)**, 1687–1697, https://doi.org/10.1175/1520-0469(1982)039<1687:ISATCD>2.0.CO;2.

Shaevitz, D. A., and Coauthors, 2014: Characteristics of tropical cyclones in high-resolution models in the present climate. *J. Adv. Model. Earth Syst.*, **6 (4)**, 1154–1172, https://doi.org/10.1002/2014MS000372.

Shen, W., 2004: Hurricane potential intensity from an energetics point of view. *Quart. J. Roy. Meteor. Soc.*, **130**, 2629–2648, https://doi.org/10.1256/qj.03.65.

Smith, R. K., and M. T. Montgomery, 2016: The efficiency of diabatic heating and tropical cyclone intensification. *Quart. J. Roy. Meteor. Soc.*, **142 (698)**, 2081–2086, https://doi.org/10.1002/qj.2804.

Smith, R. K., M. T. Montgomery, and G. Kilroy, 2018: The generation of kinetic energy in tropical cyclones revisited. *Quart. J. Roy. Meteor. Soc.*, **144 (717)**, 2481–2490, https://doi.org/10.1002/qj.3332.

Stan, C., 2012: Is cumulus convection the concertmaster of tropical cyclone activity in the Atlantic? *Geophys. Res. Lett.*, **39 (19)**, L19 716, https://doi.org/10.1029/2012GL053449.

Stansifer, E. M., P. A. O'Gorman, and J. I. Holt, 2017: Accurate computation of moist available potential energy with the Munkres algorithm. *Quart. J. Roy. Meteor. Soc.*, **143 (702)**, 288–292, https://doi.org/10.1002/qj.2921.

Tailleux, R., 2013: Available potential energy density for a multicomponent Boussinesq fluid with arbitrary nonlinear equation of state. *J. Fluid Mech.*, **735**, 499–518, https://doi.org/10.1017/jfm.2013.509.

Tailleux, R., 2018: Local available energetics of multicomponent compressible stratified fluids. *J. Fluid Mech.*, **842**, R1, https://doi.org/10.1017/jfm.2018.196.

Tang, B., and K. Emanuel, 2012: Sensitivity of Tropical Cyclone Intensity to Ventilation in an Axisymmetric Model. *J. Atmos. Sci.*, **69 (8)**, 2394–2413, https://doi.org/10.1175/JAS-D-11-0232.1.

Tang, B. H., 2010: Midlevel Ventilation's Constraint on Tropical Cyclone Intensity. Ph.D. thesis, Massachusetts Institute of Technology, URL https://dspace.mit.edu/bitstream/handle/1721.1/62321/712176836-MIT.pdf.

Trenberth, K. E., C. A. Davis, and J. Fasullo, 2007: Water and energy budgets of hurricanes: Case studies of Ivan and Katrina. *J. Geophys. Res.*, **112 (D23)**, D23 106, https://doi.org/10.1029/2006JD008303.

Tuleya, R. E., and Y. Kurihara, 1975: The Energy and Angular Momentum Budgets of a Three-Dimensional Tropical Cyclone Model. *J. Atmos. Sci.*, **32 (2)**, 287–301, https://doi.org/10.1175/1520-0469(1975)032<0287:TEAAMB>2.0.CO;2.

Vidale, P. L., and Coauthors, 2021: Impact of Stochastic Physics and Model Resolution on the Simulation of Tropical Cyclones in Climate GCMs. *J. Climate*, **34 (11)**, 4315–4341, https://doi.org/10.1175/JCLI-D-20-0507.1.

Vigh, J. L., and W. H. Schubert, 2009: Rapid Development of the Tropical Cyclone Warm Core. *J. Atmos. Sci.*, **66 (11)**, 3335–3350, https://doi.org/10.1175/2009JAS3092.1.

Wing, A. A., and Coauthors, 2019: Moist Static Energy Budget Analysis of Tropical Cyclone Intensification in High-Resolution Climate Models. *J. Climate*, **32 (18)**, 6071–6095, https://doi.org/10.1175/JCLI-D-18-0599.1.

Wong, K. C., R. Tailleux, and S. L. Gray, 2016: The computation of reference state and APE production by diabatic processes in an idealized tropical cyclone. *Quart. J. Roy. Meteor. Soc.*, **142 (700)**, 2646–2657, https://doi.org/10.1002/qj.2854.

Xue, M., and S.-J. Lin, 2001: Numerical Equivalence of Advection in Flux and Advective Forms and Quadratically Conservative High-Order Advection Schemes. *Mon. Wea. Rev.*, **129 (3)**, 561–565, https://doi.org/10.1175/1520-0493(2001)129<0561:NEOAIF>2.0.CO;2.

Yang, M.-J., S. A. Braun, and D.-S. Chen, 2011: Water Budget of Typhoon Nari (2001). *Mon. Wea. Rev.*, **139 (12)**, 3809–3828, https://doi.org/10.1175/MWR-D-10-05090.1.

Zarzycki, C. M., 2016: Tropical Cyclone Intensity Errors Associated with Lack of Two-Way Ocean Coupling in High-Resolution Global Simulations. *J. Climate*, **29 (23)**, 8589–8610, https://doi.org/10.1175/JCLI-D-16-0273.1.

Zhao, M., I. M. Held, and S.-J. Lin, 2012: Some Counterintuitive Dependencies of Tropical Cyclone Frequency on Parameters in a GCM. *J. Atmos. Sci.*, **69 (7)**, 2272–2283, https://doi.org/10.1175/JAS-D-11-0238.1.